Geologica Acta, Vol.16, Nº 3, September 2018, 293-319
DOI: 10.1344/GeologicaActa2018.16.3.4

geologica acta

Geochemistry and petrogenesis of metabasites from the Gol-e-Gohar Complex in southern Sanandaj-Sirjan metamorphic zone, South of Iran; Evidences for crustal extension and magmatism at early Palaeozoic

H. FATEHI[1] **and H. AHMADIPOUR**[1*]

[1]**Department of Geology, Faculty of Sciences, Shahid Bahonar University of Kerman**
Emam Khomeini Highway, Pajuhesh Square, Po. Box 761694111, Kerman, Iran. E-mail: hahmadi@uk.ac.ir
Tel.: +9803431322237 Fax.: +9803433257435

*Corresponding author

ABSTRACT

In Gol-e-Gohar metamorphic Complex from south-eastern Sanandaj-Sirjan metamorphic zone (Kerman province, Iran), there are two types of metabasites, wich contain layered metamorphosed lava flows and younger meta-gabbros. The protoliths formed in the Paleozoic era and were metamorphosed during the early Cimmerian orogenic phase in the late Triassic, under temperatures of 640–680ºC and pressures of ~7–10.5kbar (amphibolite facies). These rocks are garnet-bearing amphibolites, garnet-free amphibolites and metamorphosed gabbros. Many mineralogical and chemical aspects of these metabasites are similar, although the layered metabasites show tholeiitic and the meta-gabbros depict alkaline affinities. Evidences such as whole rock geochemical characteristics, Sr and Nd isotopic data, ($^{143}Nd/^{144}Nd_{initial}$=0.511913–0.512067; εNd^{550Ma}=-0.31–2.68), relatively flat patterns of chondrite-normalized Rare Earth Elements and multi-elemental diagrams, the enrichment in TiO_2 (average content ~2.16) and high Zr/Y ratios (3–8), indicate that all of Gol-e-Gohar metabasites were formed in an extensional intra-continental rift zone from tholeiitic to alkaline magmas. The data suggest that the parent magmas could derive from low degrees of partial melting of spinel-lherzolite sources in subcontinental lithospheric mantle. These evidences confirm the existence of extensional environments in the southern part of the Sanandaj-Sirjan metamorphic zone in the Paleozoic era, when large extensional depressions developed in the Sanandaj-Sirjan metamorphic zone with underlying asthenosphere ascent. Partial melting took place during this time. Gradually, thick sequences of continental detritic sediments and tholeiitic lava flows accumulated in these troughs. A subsequent magmatic event in the area was characterized by emplacement of alkaline gabbro intrusions. At the early Cimmerian orogeny, these sedimentary-igneous rock associations metamorphosed and the Gol-e-Gohar metabasites formed.

KEYWORDS **Metabasite. Sanandaj-Sirjan metamorphic zone. Iran. Gol-e-Gohar Complex.**

INTRODUCTION

Metamorphosed basic and ultrabasic rocks are important to understand the tectonic evolution of orogenic belts. These rocks usually represent locations where subduction of oceanic lithosphere took place before continental collision. Four different aspects need to be addressed to understand the significance of basic rocks in orogenic belts: i) the age of protolith and metamorphism; ii) geochemistry; iii) metamorphic evolution and iv) structural evolution. In particular, the geochemical features of these rocks, together with the protolith age,

can be used to characterize the pre-collisional history of the orogens in the tectonic scenario where the basic rocks were formed, for example, large or narrow ocean, back-arc basin, continental rift, subduction zone, etc. In this respect, the recognition of remains of ophiolitic sequences is of particular interest. The study of the metamorphic and structural evolution of basic rocks provides information on possible subduction events responsible for the closure of an intervening ocean, as well as on the subsequent exhumation of these rocks after the collision. The reconstruction of pre-collisional tectonic settings for Palaeozoic or older orogenic belts based on the analysis of basic rocks contains more uncertainties than the recnstruction for younger belts. These difficulties usually arise from uncertainties concerning the age of the protoliths along with complicated metamorphic and structural evolutions and sometimes polyorogenic histories. These agents may obliterate the primary geochemical signatures of the rocks. Despite these limitations, a careful and systematic geochemical study of the basic rocks included in the orogenic belts, together with other geological and isotopic data, can be regarded as a powerful tool to produce well-supported and coherent tectonic reconstructions in relevant areas. Therefore, understanding the magmatic evolution of metamorphosed basic rocks and their metamorphic conditions might clarify the geodynamical processes that modified the crust in older eras (Maruyama *et al*., 1996; Bruand *et al*., 2011).

Petrological characteristics and temperature and pressure estimations of metamorphic rocks in the northern part of the Sanandaj-Sirjan metamorphic zone have been discussed by several authors (*e.g*. Sheikholeslami *et al*., 2003, 2008; Baharifar *et al*., 2004; Sepahi *et al*., 2004; Saki *et al*., 2011). Additionally, Mohajjel and Fergusson (2000, 2014), Mohajjel *et al*. (2003, 2006), Ahmadi Khalaji *et al*. (2007) and Mahmoodi *et al*. (2011) studied thermal and tectonic events in the northern part of the Sanandaj-Sirjan metamorphic zone. But, the thermal and metamorphic events of the southern Sanandaj-Sirjan metamorphic zone, especially the petrology and structure of the metabasites, have been neglected. In the south-eastern of Sanandaj-Sirjan metamorphic zone (South of Iran), there are some metabasite associations, which represent magmatic activities in this part of Iran in the Palaeozoic, whose investigation can help to clearify the geological evolution of the Iranian platform at that time. The aim of this paper is to present the field and petrographical characteristics of these rocks, along with their geochemical and isotopic characteristics and petrogenesis to understand their tectonic setting.

GEOLOGICAL SETTING

The study area is located in the South-East of Iran (Kerman Province), in the south-eastern part of Sanandaj-Sirjan metamorphic zone (Fig. 1). This zone is a hinterland in the Zagros Orogeny (Mohajjel and Fergusson, 2000) and contains weakly to intensely metamorphosed and deformed Palaeozoic rocks. The Zagros Orogeny originated from the closure of the Neo-Tethys following the complete consumption of oceanic crust along a northeast-dipping subduction zone and subsequent continental collision between the Afro-Arabian and Iranian continental fragments (Mohajjel and Fergusson, 2000, 2014; Mohajjel *et al*., 2003; Agard *et al*., 2005, 2011). This orogenic belt from South-West to North-East includes: i) the Mesopotamian-Persian Gulf foreland basin; ii) the Zagros fold-thrust belt; iii) the Sanandaj-Sirjan metamorphic zone (Stocklin, 1968) and iv) the Urumieh-Dokhtar magmatic arc. The Sanandaj-Sirjan metamorphic zone and Urumieh-Dokhtar magmatic arc, to the North-East of the main Zagros thrust, are presumed to be the result of a northeast-dipping subduction process linked to the subduction of Neo-Tethys oceanic crust beneath the Iranian continental active margin (Omrani, 2008).

The Sanandaj-Sirjan metamorphic zone has 150–250km-width and 1500km-long, stretching from SE Iran to NE Iraq, where it joins to the Taurus Belt in Turkey (Mohajjel and Fergusson, 2000, 2014; Mohajjel *et al*., 2003; Agard *et al*., 2005, 2011). Apart from the Palaeozoic rocks, this zone contains deformed and undeformed Mesozoic plutons and volcanic rocks (Mohajjel *et al*., 2003; Ahmadi Khalaji *et al*., 2007; Ghalamghash *et al*., 2009;Mahmoodi *et al*., 2011). This metamorphic complex has been divided into two parts, northern and southern (Mohajjel *et al*., 2003). The northern Sanandaj-Sirjan metamorphic zone is dominated by Triassic-Jurassic rocks and, in places, Cretaceous turbidites, originally deposited as deep submarine fans, are preserved and intruded by plutons (Ghalamghash *et al*., 2009). This northern zone was deformed and metamorphosed in the late Jurassic-early Cretaceous (Ghalamghash *et al*., 2009) (Fig. 1A). The southern Sanandaj-Sirjan metamorphic zone contains Palaeozoic rocks, which were formed in a cratonic environment, and Permian-Carboniferous mafic-ultramafic rocks. In the South of the Sanandaj-Sirjan metamorphic zone, the Palaeozoic units were deformed and metamorphosed during the early Cimmerian orogeny in the late Triassic (Sheikholeslami, 2008; Arfania and Shahriari, 2009). Structures associated with the early Cimmerian orogenic phase are S-SW verging folds and deformed under low-grade green-schist to amphibolite metamorphic conditions (Mohajjel *et al*., 2003). The study area is located in the southern part of this metamorphic complex and contains the Palaeozoic metamorphic rocks of the Gol-e-Gohar, Rutchun and Khabr complexes. Stratigraphically, Gol-e-Gohar is the lower unit and consists of Cambrian slates, phyllites, micachists, gneisses, metabasites (metamorphosed basic lava flows

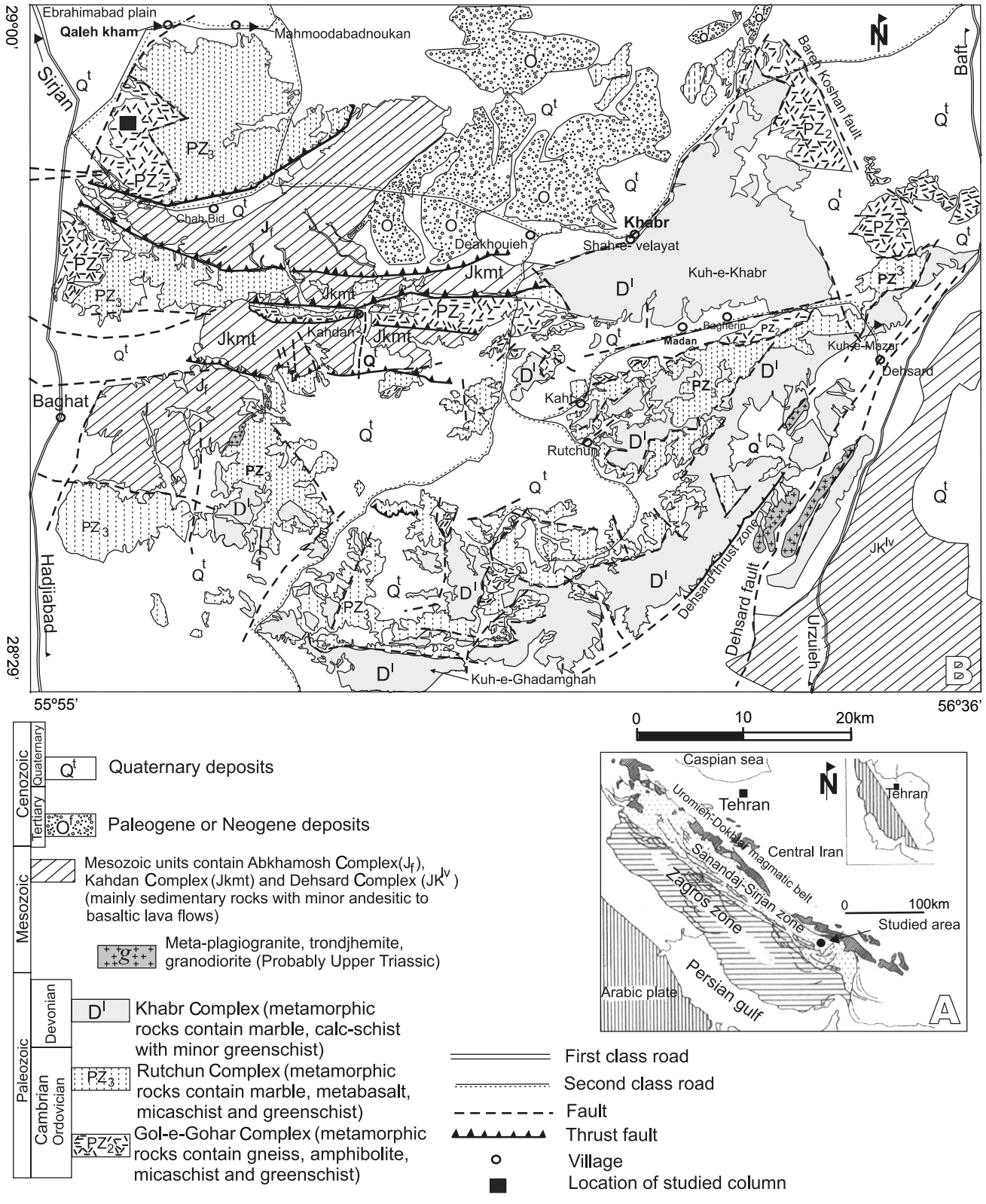

FIGURE 1. A) Geological situation of the study area in Iran (Mohajjel and Fergusson, 2000). B) Simplified geological map of the study area (Sabzehei *et al.*, 1997b) showing the location of the stratigraphic column in Figure 3.

and intrusions) and quartzites (Sabzehei *et al*., 1997). This unit is overlain by the Ordovician Rutchun Complex which contains meta-dolomites, greenschists and mica-schists (Sabzehei *et al*., 1997). In certain areas, a middle Devonian-eraly Carboniferous suite of marbles, calc-schists, slates and phyllites (Khabr complex), overlies the Rutchun Complex. Unmetamorphosed Mesozoic units consist of shales, sandstones, conglomerates and basaltic to andesitic lava flows. These units are mainly present in the northern part of the study area (Fig. 1) (Sabzehei *et al*., 1997; Fatehi *et al*., 2017).

ANALYTICAL METHODS

In order to investigate detail petrographical and geochemical charateristics, a total of 50 samples were collected from five outcrops of metabasites in the Gol-e-Gohar Complex. The samples took from the lowest metamorphic grade rocks (Sample GB-107) to the higher grades. The higher grade samples include garnet bearing metamorphosed lava flows (GB-93, GB-103, GB-104 and GB-259), garnet-free metamorphosed lava flows (GB-38, GB-107 and GB-120) and garnet-free metamorphosed gabbro intrusions (GB-96 and GB-181). These samples were analysed in the ALS Chemex Laboratory Group Ltd, B.C., Canada, for whole rock major, trace and Rare Earth Element (REE).

Major elements were determined by lithium meta-borate fusions HNO_3 total digestion, by an Inductively-Coupled Plasma-Atomic Emission Spectrometer (ICP-AES (ME-ICP-06)) with a detection limit of 0.01%, (Table 1), and trace elements were determined analysing pressed powder pellets by an Inductively-Coupled Plasma-Mass Spectrometer (ICP-MS (ME-MS81)) with detection limit of 0.01ppm. Loss On Ignition (LOI) was determined by heating a separate aliquot of rock powder at 900ºC for >2h. Analytical error for most elements was less than 2%.

Polished thin sections of samples were investigated by transmitted and reflected light microscopy. Three polished-thin sections (GB-38, GB-93 and GB-259) were selected and prepared for electron microprobe analyses based on their petrography and mineral paragenesis. In these polished thin sections, garnet, amphibole, ilmenite, biotite, plagioclase and quartz were analysed (Tables 2–5). The chemical composition of minerals in the metabasites were obtained using a JEOL JXA-8600M Electron Probe Micro Analysis (EPMA) at the EMS Laboratory of Yamagata University in Japan with an accelerating voltage of 15kV and a beam current of 20nA and count times of 10 seconds. Natural and synthetic materials were used as standards. The detection limits for the elements analysed are between 0.02 and 0.09%. Major element mapping of garnet, amphibole and plagioclase was also re-analysed to check whether or not the analysed spots were representative of the chemical composition and zoning. Abbreviations for mineral names used in the text, figures and tables are from Whitney and Evans (2010).

The $^{87}Sr/^{86}Sr$ and $^{143}Nd/^{144}Nd$ isotopic ratios and trace element concentrations of Rb, Sr, Sm and Nd were measured by a Multi-Collector Thermal Ionisation Mass Spectrometer (TIMS) VG Sector 54 on 4 whole rock samples, GB-38, GB-93, GB-103 and GB-259, in the Isotope Geological Laboratory at Aveiro University (Portugal) (Table 6). Samples were dissolved with HF/HNO_3 in Teflon Parr acid digestion bombs at 200ºC. After evaporation of the final solution, the samples were dissolved with HCl (6N) and dried down. The elements for analysis were purified using a conventional two-stage ion chromatography technique: i) separation of Sr and REE elements in ion exchange column with AG8-50 W Bio-Rad cation exchange resin; ii) purification of Nd from other lanthanide elements in columns with Ln (El Chrom Technologies) cation exchange resin. All reagents used in sample preparation were sub-boiling distilled, and the water was produced by a Milli-Q Element (Millipore) apparatus. Sr was loaded on a single Ta filament with H_3PO_4, whereas Nd was loaded on a Ta side filament with HCl, in a triple filament arrangement. Data were obtained in dynamic mode with peak measurements at 1–2V for ^{88}Sr and 0.8–1.5V for ^{144}Nd. Sr and Nd isotopic ratios were corrected for mass fractionation relative to $^{88}Sr/^{86}Sr=0.1194$ and $^{146}Nd/^{144}Nd=0.7219$.

RESULTS

Field relationships

The Gol-e-Gohar metamorphic Complex (Fig. 2A) contains metasedimentary rocks (slates, phyllites and micaschists), metabasites (amphibole-schists, amphibolites, garnet metabasites (Fig. 2B) and garnet-free metabasites (Fig. 2C, D)), metamorphosed acidic igneous rocks and meta-limestones, that underwent three metamorphic events and four deformation phases (Sabzehei *et al*., 1997; Fatehi *et al*., 2017). The metasedimentary units occur as layers of variable thicknesses (from 0.2m up to 100m) which have been intruded by metamorphosed gabbroic and acidic igneous rocks. The metabasite layers can be up to 100m in thickness. They alternate with micaschist layers and are cut by small garnet-free metamorphosed gabbroic apophyses (Fig. 2E).

A detailed field description of these units are presented as a stratigraphic column in Figure 3. The column is located in the South of Qaleh Kham village (55º58'19"N,

TABLE 1. Geochemical composition of metabasites from Gol-e-Gohar metamorphic Complex

Sample	GB-103	GB-93	GB-107	GB-120	GB-259	GB-104	GB-38	GB-181	GB-96
Rock Type	Grt Am(Met)	Grt Am(Met)	Am (Met)	Am (Met)	Grt Am(Met)	Grt Am(Met)	Am (Met)	Am (Gab)	Am (Gab)
SiO_2 (wt.%)	49.6	51.3	48.7	49.4	46.9	54.1	50.5	47.9	52.4
TiO_2	2.02	3.4	2.66	1.55	3.29	2.37	1.32	1.94	1.84
Al_2O_3	14.8	13.6	13.3	15.45	15.4	14.2	15.05	16.2	16.65
FeO_t	13.2	16.5	13.5	11.45	16.45	13.8	10.85	10.1	8.47
MgO	5.99	4.57	5.02	6.91	5.59	4.43	6.53	5.94	4.67
CaO	7.93	7.11	8.28	9.11	8.5	6.69	8.42	6.95	5.33
MnO	0.22	0.2	0.22	0.2	0.26	0.22	0.09	0.08	0.06
Na_2O	2.55	2.33	3.1	2.93	2.42	2.46	4.92	4.26	4.2
K_2O	1.29	0.33	0.88	1.11	0.39	1.58	0.86	2.15	3.18
Cr_2O_3	0.03	0.01	0.01	0.03	0.01	0.01	0.03	<0.01	0.01
P_2O_5	0.29	0.62	0.38	0.16	0.53	0.34	0.2	0.23	0.12
SrO	0.01	0.02	0.02	0.03	0.02	0.01	0.01	0.06	0.07
BaO	0.02	0.01	0.01	0.02	0.01	0.05	0.01	0.04	0.07
LOI	1.6	1.14	1.93	2.67	1.01	1.53	1.89	3.34	2.57
Total	99.55	101.14	98.01	101.02	100.78	101.79	100.68	99.19	99.64
Mg#	0.45	0.33	0.4	0.52	0.38	0.36	0.52	0.51	0.5
Ba (ppm)	206	106	94.8	163	84.9	449	108	328	622
Rb	31.4	5.7	19.1	32.5	6.3	45.6	24.3	58.6	98.6
Sr	112	167.5	183.5	277	177.5	126.5	188	556	580
Cr	180	100	40	190	60	40	230	10	60
Cs	1.16	0.16	0.72	0.72	0.15	1.6	0.74	60.6	8.73
Ga	22.4	23.2	22	19.5	24.5	20.8	18.7	18.8	18.2
Hf	4.2	6.8	6.4	3.2	6.3	3.9	2.7	3.3	3.2
Nb	14.3	21.2	18.7	6.9	32.9	6.4	7.1	39.8	38.9
Nd	23.4	39	31.5	22.2	34.4	21.9	21.4	22.6	12.7
Ni	51	8	24	19	59	18	42	56	28
Sn	21	11	3	2	4	29	3	3	2
Ta	0.9	1.4	1.2	0.4	2	0.4	0.4	2.5	2.5
Th	2.93	3.9	3.35	2.36	2.84	3.28	1.51	5.01	1.95
U	1.03	1.54	0.88	0.73	0.92	1.17	1.38	0.84	0.7
V	301	371	343	311	288	366	252	180	164
W	22	<1	1	1	1	33	1	<1	1
Y	38.7	42.8	47.3	27.7	32.4	37.7	29.6	21.3	15.1
Zr	162	277	251	121	267	139	104	132	129
La	17.9	30.1	22.5	16.5	28.7	16.2	20.7	21.3	11.3
Ce	36.4	65.1	50.1	35.8	60.4	33.8	43	42.2	23.4
Pr	4.94	8.56	6.85	4.75	7.73	4.66	5.11	5.26	3.02
Nd	23.4	39	31.5	22.2	34.4	21.9	21.4	22.6	12.7
Sm	5.68	9.29	7.91	5.17	8.12	5.7	5.17	5.15	3.4
Eu	1.78	2.78	2.27	1.81	2.48	2.03	1.84	1.65	1.1
Gd	6.54	9.65	8.94	5.78	7.73	6.62	5.73	5.38	3.27
Tb	1.13	1.51	1.44	0.93	1.19	1.07	0.93	0.8	0.51
Dy	7.08	8.15	8.64	5.69	6.57	6.84	5.36	4.36	3.05
Ho	1.53	1.8	1.85	1.14	1.27	1.48	1.18	0.87	0.6
Er	4.2	4.6	4.89	2.9	3.23	4.12	3.12	2.17	1.69
Tm	0.64	0.69	0.78	0.46	0.47	0.65	0.49	0.33	0.26

TABLE 1. (Cont.)

Sample	GB-103	GB-93	GB-107	GB-120	GB-259	GB-104	GB-38	GB-181	GB-96
Yb	3.95	4.17	4.71	2.8	2.93	4.04	3.02	1.87	1.54
Lu	0.6	0.66	0.74	0.41	0.44	0.58	0.46	0.27	0.24
Nb/Y	0.37	0.5	0.4	0.25	1.02	0.17	0.24	1.87	2.58
Ce/Y	0.94	1.52	1.06	1.29	1.86	0.9	1.45	1.98	1.55
Zr/Y	4.19	6.47	5.31	4.37	8.24	3.69	3.51	6.2	8.54
Ti/Y	312.93	476.25	337.15	335.47	608.77	376.89	267.35	546.04	730.54
Zr/Nb	11.33	13.07	13.42	17.54	8.12	21.72	14.65	3.32	3.32
$(La/Sm)_N$	1.94	2	1.76	1.97	2.18	1.75	2.47	2.55	2.05
Sm/Yb	1.44	2.23	1.68	1.85	2.77	1.41	1.71	2.75	2.21
$(Nb/Nb^*)_{pm}$	0.72	1.01	1.13	0.41	1.71	0.2	0.44	1.43	1.03
$(Ce/Yb)_N$	2.34	3.97	2.71	3.25	5.24	2.13	3.62	5.74	3.86
$(Dy/Yb)_N$	1.15	1.25	1.18	1.3	1.44	1.09	1.14	1.5	1.27
La/Ta	19.89	21.5	18.75	41.25	14.35	40.5	51.75	8.52	4.52
La/Nb	1.25	1.42	1.2	2.39	0.87	2.53	2.92	0.54	0.29
Yb_N	17.95	18.95	21.41	12.73	13.32	18.36	13.73	8.5	7

Abbreviations= Grt: Garnet; Am: Amphibolite; Met: Metabasite; Gab: Gabbro; LOI: Loss On Ignition; wt.%: weight percent; ppm: parts per million; FeO_T is total iron as FeO; Mg# = mol MgO/MgO+FeO.

28º56'26"E) and the layers show a strike of N80W and dip of 55NE. In this column, the measurments have been done perpendicular to the strike of the layers from the older units to the younger ones.

The lowermost part of the column consist of garnet amphibolites (unit 1, Figs. 2B; 3) which contain garnet euhedral porphyroblasts (up to 1.5cm in diameter), amphibole and plagioclase with ribbon to granoblastic texture. This unit is followed by a micaschist and garnet-free metabasite layers (unit 3, Figs. 2C, D; 3). Upwards, a successions of metabasites, meta-pelites and meta-limestones occur and then, ribbon textured metamorphosed garnet-free metabasites appear. The latter units contain coarse-grained amphibole and plagioclase porphyroblasts (Figs. 3; 4B). The contact between the Gol-e-Gohar and Rutchun complexes is a normal fault. Metamorphosed ribbon textured gabbros containing coarse amphibole and plagioclase (Fig. 2E) intrude the metabasites, mostly in the lower parts of the column. These intrusions show dark amphibole-rich and light plagioclase-rich bands. In the upper part of the column, the metabasite and metapelite layers cut by metamorphosed acidic intrusions.

Metabasites, occur as dark colored layers of variable thicknesses (from 1m to more than 200m) alternating with slates, phyllites, schists and meta-limestones. In the middle part of the studied area (South of Deakhouieh village), low-grade fine-grained metabasites (Sample GB-107) show a weakly-developed foliation (Árkai *et al.*, 2002; Best, 2002) and primary porphyritic texture with residual magmatic plagioclase crystals. With the increase of the metamorphic grade, crystal coarsening and metamorphic differentiation happened and new schistosity appear as separated dark amphibole-rich and light plagioclase-rich bands (Fig. 2C). In the low metamorphic-grade samples, the main minerals are actinolite-hornblende crystals (up to 3mm–length) and epidote and chlorite (with up to 1mm-length), while in higher-grade samples, the sizes of hornblende and plagioclase crystals reach 15 up to 20mm and chlorite and epidote mainly removed from the metabasites.

Petrography

Next, the relation between metamorphic events and deformation phases in the rock units of the area, is briefly described. In the first metamorphic event, which was associated with the first deformation phase, muscovite, biotite and garnet minerals were formed and oriented along the first schistosity (S_1) just parallel to the F_1 axial plane. The second metamorphic event acted simultaneously with the second deformation phase and led to the overgrowth of the porphyroblasts and re-orientation of them parallel to the second schistosity, parallel to the F_2 exial plane. The third metamorphic event in association with the third deformation phase produced mylonitic structures (local S_3 foliation). The last deformation phase produced normal, reverse, and thrust faults in a brittle condition.

Low grade metabasites from the middle part of the studied area (middle to lower greenschist facies, sample GB-107) are defined by remnants of magmatic plagioclase and pyroxene crystals and primary porphyritic texture. In these samples, minerals such as epidote, chlorite and actinolite-

TABLE 2. Representative analyses of hornblendes in Gol-e-Gohar metabasites

Rock Type	Metabasite (Amphibolite)											
Phase	hornblende											
SiO_2 (wt.%)	43.19	42.96	43.54	43.44	43.48	43.37	42.94	42.77	43.03	43.37	42.65	43.92
TiO_2	0.76	0.82	0.79	0.73	0.73	0.56	0.66	0.71	0.64	0.65	0.55	0.64
Al_2O_3	14.3	14.56	14.37	14.8	14.69	15.03	15.33	14.62	15.08	15.54	15.78	16.37
FeO	18.35	18.36	17.91	17.7	16.14	17.95	17.9	17.16	17.32	15.81	16.33	15.93
MnO	0.07	0.12	0.1	0.07	0.06	0.05	0.1	0.13	0.11	0.14	0.08	0.05
MgO	8.78	8.72	9	8.74	8.86	8.71	8.33	8.57	8.71	9.69	8.98	9.66
CaO	10.79	11.12	11.17	11.18	11.07	11.03	10.9	11.05	11.03	11.04	11.11	11.06
Na_2O	1.85	2	1.77	1.73	1.87	1.98	1.94	2	1.94	1.63	1.56	1.67
K_2O	0.45	0.36	0.38	0.35	0.43	0.3	0.34	0.36	0.3	0.44	0.48	0.52
F	0.23	0	0	0.13	0	0.04	0.02	0.08	0.31	0	0.13	0
Cl	0.03	0.1	0.06	0.04	0.01	0.03	0.07	0.04	0.02	0.05	0.04	0.07
Total	98.8	99.12	99.1	98.9	97.35	99.04	98.53	97.5	98.49	98.35	97.69	99.89
Formula	23 O											
Si	6.29	6.26	6.32	6.32	6.41	6.3	6.27	6.33	6.29	6.27	6.25	6.24
Ti	0.08	0.09	0.09	0.08	0.08	0.06	0.07	0.08	0.07	0.07	0.06	0.07
Al^{iv}	1.71	1.74	1.68	1.68	1.59	1.7	1.73	1.67	1.71	1.73	1.75	1.76
Al^{vi}	0.75	0.76	0.78	0.86	0.97	0.87	0.91	0.88	0.89	0.91	0.97	0.98
Fe^{3+}	0.8	0.69	0.68	0.62	0.34	0.67	0.64	0.48	0.61	0.72	0.65	0.71
Fe^{2+}	1.44	1.54	1.49	1.53	1.65	1.51	1.55	1.65	1.51	1.19	1.35	1.18
Mn	0.01	0.01	0.01	0.01	0.01	0.01	0.01	0.02	0.01	0.02	0.01	0.01
Mg	1.91	1.89	1.95	1.89	1.95	1.88	1.81	1.89	1.9	2.09	1.96	2.05
Ca	1.69	1.74	1.74	1.74	1.75	1.72	1.71	1.75	1.73	1.71	1.74	1.68
Na	0.52	0.57	0.5	0.49	0.53	0.56	0.55	0.57	0.55	0.46	0.44	0.46
K	0.08	0.07	0.07	0.07	0.08	0.05	0.06	0.07	0.06	0.08	0.09	0.09
F	0.11	0	0	0.06	0	0.02	0.01	0.04	0.14	0	0.06	0
Cl	0.01	0.02	0.01	0.01	0	0.01	0.02	0.01	0	0.01	0.01	0.02
Total	15.39	15.38	15.32	15.36	15.36	15.35	15.35	15.44	15.47	15.26	15.34	15.26
$Mg/(Mg+Fe^{2+})$	0.57	0.55	0.57	0.55	0.54	0.56	0.54	0.53	0.56	0.64	0.59	0.63

TABLE 3. Representative analyses of garnets in Gol-e-Gohar metabasites

Rock Type	Metabasite (Amphibolite)											
Sample	GB-93						GB-259					
Phase	Garnet											
part	Core	Rim	Rim	Core	Core	Rim	Core	Mid	Rim	Core	Mid	Rim
SiO_2 (wt.%)	39.05	39.23	39.32	38.42	38.29	38.89	38.37	38.2	37.69	38.18	38.36	38.68
TiO_2	0.07	0.06	0.06	0.01	0.12	0.07	0.11	0.12	0.08	0.15	0.16	0.06
Al_2O_3	21.96	21.88	21.26	21.64	21.5	21.7	21.48	21.35	21.31	21.6	21.96	21.81
Cr_2O_3	0.05	0	0	0	0	0	0.06	0.05	0	0	0	0.01
FeO	30.68	28.94	28.99	30.37	28.84	30.19	27.66	27.02	28.22	28.29	28.32	28.63
MnO	1.97	0.98	0.97	2.89	2.67	0.89	4.31	4.31	0.94	3.49	2.24	1.74
MgO	2.72	3.07	3.08	2.53	2.27	3.13	2	2.02	2.64	1.92	2.21	2.56
CaO	6.29	7.36	7.4	6.24	6.79	7.2	8.16	8.15	8.14	8.1	8.2	8.33
Na_2O	0	0	0	0.03	0.03	0	0.02	0.06	0.06	0.05	0.06	0.06
K_2O	0	0.01	0.02	0.02	0.01	0	0	0	0.01	0	0	0
F	0.08	0	0	0	0.06	0	0.32	0.3	0	0.18	0.12	0
Cl	0	0	0	0.01	0.02	0	0	0	0.02	0	0	0.01
Total	102.87	101.51	101.1	102.16	100.6	102.08	102.5	101.6	99.13	101.96	101.65	101.87
Formula	12 O											
Si	3.03	3.06	3.08	3.01	3.04	3.02	3	3.01	3.02	3	3.01	3.02
Ti	0	0	0	0	0.01	0	0.01	0.01	0.01	0.01	0.01	0
Al	2.01	2.01	1.97	2	2.01	1.99	1.98	1.98	2.01	2	2.03	2
Cr	0	0	0	0	0	0	0	0	0	0	0	0
Fe^{3+}	0	0	0	0	0	0	0	0	0	0	0	0
Fe^{2+}	1.99	1.89	1.9	1.99	1.91	1.96	1.8	1.78	1.89	1.86	1.86	1.87
Mn	0.13	0.06	0.06	0.19	0.18	0.06	0.29	0.29	0.06	0.23	0.15	0.11
Mg	0.31	0.36	0.36	0.29	0.27	0.36	0.23	0.24	0.32	0.22	0.26	0.3
Ca	0.52	0.62	0.62	0.52	0.58	0.6	0.68	0.69	0.7	0.68	0.69	0.7
Total	8	8	8	8	8	8	8	8	8	8	8	8
X_{alm}	0.67	0.65	0.65	0.66	0.65	0.66	0.6	0.59	0.64	0.62	0.63	0.63
X_{prp}	0.11	0.12	0.12	0.1	0.09	0.12	0.08	0.08	0.11	0.08	0.09	0.1
X_{grs}	0.18	0.21	0.21	0.17	0.2	0.2	0.23	0.23	0.24	0.23	0.23	0.23
X_{spess}	0.04	0.02	0.02	0.06	0.06	0.02	0.09	0.1	0.02	0.08	0.05	0.04
X_{Fe}	0.86	0.84	0.84	0.87	0.88	0.84	0.89	0.88	0.86	0.89	0.88	0.86

TABLE 4. Representative analyses of plagioclases in Gol-e-Gohar metabasites

Rock Type						Metabasite (amphibolite)						
Phase						Plagioclase						
SiO_2 (wt.%)	63.74	63.16	62.87	62.87	63.39	64.09	62.2	63.1	61.47	62.09	62.1	63.19
TiO_2	0	0	0	0	0	0.02	0	0.05	0.02	0.03	0	0
Al_2O_3	23.8	23.84	23.68	23.17	24.12	24.08	23.8	23.99	24.19	23.98	23.95	23.64
Cr_2O_3	0	0	0.01	0.01	0	0	0	0	0.02	0	0	0
Fe_2O_3	0	0	0.12	0.07	0.02	0	0	0.04	0.03	0.05	0.09	0.02
FeO	0	0	0	0	0	0	0	0	0	0	0	0
MnO	0	0.02	0	0	0	0.01	0.01	0.05	0.06	0	0.05	0.01
MgO	0	0	0	0.01	0.01	0	0.01	0.01	0	0	0	0.02
CaO	4.79	4.98	4.6	4.52	5.1	4.96	5.17	5.03	4.81	5.5	5.14	4.95
Na_2O	9.27	9.1	9.36	9.33	9.33	9.26	8.71	8.93	8.14	8.47	8.63	8.91
K_2O	0.07	0.05	0.03	0.1	0.05	0.04	0.08	0.07	1.27	0.04	0.06	0.04
F	0.02	0.02	0.16	0	0.07	0	0.02	0.16	0.07	0	0	0.09
Cl	0.03	0	0.02	0.04	0.02	0	0.01	0.03	0	0.02	0	0.01
Total	101.72	101.17	100.86	100.12	102.1	102.47	100.01	101.45	100.08	100.18	100.01	100.87
Formula						8 O						
Si	2.77	2.76	2.77	2.78	2.76	2.77	2.76	2.76	2.74	2.76	2.77	2.77
Ti	0	0	0	0	0	0	0	0	0	0	0	0
Al	1.22	1.23	1.23	1.21	1.24	1.23	1.24	1.24	1.27	1.25	1.27	1.24
Cr	0	0	0	0	0	0	0	0	0	0	0	0
Fe^{3+}	0	0	0	0	0	0	0	0	0	0	0	0
Fe^{2+}	0	0	0	0	0	0	0	0	0	0	0	0
Mn	0	0	0	0	0	0	0	0	0	0	0	0
Mg	0	0	0	0	0	0	0	0	0	0	0	0
Ca	0.22	0.23	0.22	0.21	0.24	0.23	0.25	0.24	0.23	0.26	0.24	0.23
Na	0.78	0.77	0.8	0.8	0.79	0.78	0.75	0.76	0.7	0.73	0.74	0.76
K	0	0	0	0.01	0	0	0	0	0.07	0	0	0
Total	5	5	5.02	5.01	5.02	5.01	5	5	5.01	5	5.03	5.01
An	22.12	23.16	21.3	21.01	23.14	22.77	24.59	23.64	22.84	26.35	24.67	23.42
Ab	77.49	76.57	78.51	78.45	76.61	77.01	74.95	75.99	69.95	73.42	75	76.36
Or	0.39	0.27	0.19	0.54	0.25	0.22	0.46	0.37	7.2	0.23	0.33	0.22

TABLE 5. Representative analyses of biotite and ilmenite in Gol-e-Gohar metabasites

Rock Type	Metabasite									
Phase	Biotite					Ilmenite				
SiO_2 (wt.%)	36.96	36.87	35.98	35.45	36.77	0	0	0	0	0.74
TiO_2	1.57	1.62	1.52	1.5	1.44	48.27	48.16	48.49	48.78	49.57
Al_2O_3	16.18	15.65	15.95	15.84	16.38	0.02	0	0	0.02	0.09
Cr_2O_3	0.07	0.02	0	0	0	0	0	0	0	0.02
FeO	17.38	17.17	18.65	17.42	16.44	46.74	45.84	46.01	46.23	45.07
MnO	0.05	0.04	0.01	0.01	0	0.49	0.59	0.48	0.46	0.44
MgO	12.08	11.61	12.23	12.31	12.79	0.07	0.19	0.2	0.22	0.28
CaO	0.59	0.41	0.6	0.4	0.47	0.07	0.04	0	0	0.62
Na_2O	0.12	0.09	0.1	0.09	0.09	0	0.07	0.04	0	0
K_2O	6.29	6.64	5.93	5.83	5.79	0.03	0	0	0	0
F	0.2	0.18	0	0.06	0.34	0	0.04	0	0.21	0
Cl	0.08	0.11	0.13	0.08	0.07	0.01	0	0.01	0	0
Total	91.58	90.4	91.1	88.99	90.59	95.72	94.93	95.23	95.94	96.84
Formula	11 O					6 O				
Si	2.81	2.85	2.78	2.79	2.81	0	0	0	0	0.04
Ti	0.09	0.09	0.09	0.09	0.08	1.94	1.95	1.95	1.95	1.94
Al^{iv}	1.19	1.15	1.22	1.21	1.19					
Al^{vi}	0.27	0.27	0.23	0.27	0.29					
Al_t	1.45	1.43	1.45	1.47	1.48	0	0	0	0	0.01
Cr	0	0	0	0	0	0	0	0	0	0
Fe	1.11	1.11	1.21	1.15	1.05	2.09	2.06	2.06	2.06	1.96
Mn	0	0	0	0	0	0.02	0.03	0.02	0.02	0.02
Mg	1.37	1.34	1.41	1.45	1.46	0.01	0.02	0.02	0.02	0.02
Ca	0.05	0.03	0.05	0.03	0.04	0	0	0	0	0.03
Na	0.02	0.01	0.02	0.01	0.01	0	0.01	0	0	0
K	0.61	0.65	0.58	0.59	0.57	0	0	0	0	0
F	0.05	0.04	0	0.02	0.08					
Cl	0.01	0.01	0.02	0.01	0.01					
Total	7.58	7.58	7.6	7.61	7.59	4.06	4.06	4.05	4.05	4.02
Fe/(Fe+Mg)	0.45	0.45	0.46	0.44	0.42	1	0.99	0.99	0.99	0.99
Mg/(Mg+Fe)	0.55	0.55	0.54	0.56	0.58	0	0.01	0.01	0.01	0.01

hornblende represent the post magmatic ferromagnesian minerals and the primary feldspars have changed into chlorite, sericite and calcite (Fig. 4A). The modal composition of garnet-free metabasites (amphibolites) is: hornblende (45%), plagioclase (30%), quartz (3–7%), epidote (1–4%), biotite (2–6%), titanite (0–2%) and other opaque minerals (1–2%). In these rocks, it is possible to observe a coarsening of the crystals coincident with a reduction in the percentage of biotite and epidote of 80% and 90%, respectively. Moreover, the texture tends to be more granoblastic (Fig. 4B). The modal composition of garnet-bearing metabasites (garnet amphibolite) is: garnet (10–15%), hornblende (45%), plagioclase (20%), quartz (2–5%), epidote (0–3%), biotite (0–4%), titanite (0–2%) and other opaque minerals (1–2%) (Fig. 4C). These rocks also show a granoblastic texture and a decrease in the percentage of edidote and biotite of 95–100% and 90–100%, respectively, coincident with the increment of the metamorphic grade. The metamorphosed gabbroic intrusions are free of garnet and consist of 55% hornblende

TABLE 6. Whole rock isotopic data for Gol-e-Gohar metabasites

Sample	Sr(ppm)	Rb(ppm)	$^{87}Rb/^{86}Sr(m)$	$^{87}Sr/^{86}Sr(m)$	$^{87}Sr/^{86}Sr(i)$	eSr(i)	Nd(ppm)	Sm(ppm)	$^{147}Sm/^{144}Nd(m)$	$^{143}Nd/^{144}Nd(m)$	$^{143}Nd/^{144}Nd(i)$	eNd(i)
GBA-103	112	31.4	0.812	0.721457	0.715088	159.64	23.4	5.68	0.147	0.512493	0.511963	0.67
GBA-93	168	5.7	0.098	0.710561	0.709791	84.38	39	9.29	0.144	0.512536	0.512017	1.71
GB-259	178	6.3	0.102	0.70914	0.708337	63.72	34.4	8.12	0.143	0.512581	0.512067	2.68
GB-38	188	24.3	0.374	0.711169	0.708236	62.29	21.4	5.17	0.146	0.51244	0.511913	-0.31

Element concentrarions were determined by ICM-MS. Sr and Nd were calculated assuming age of 550Ma.

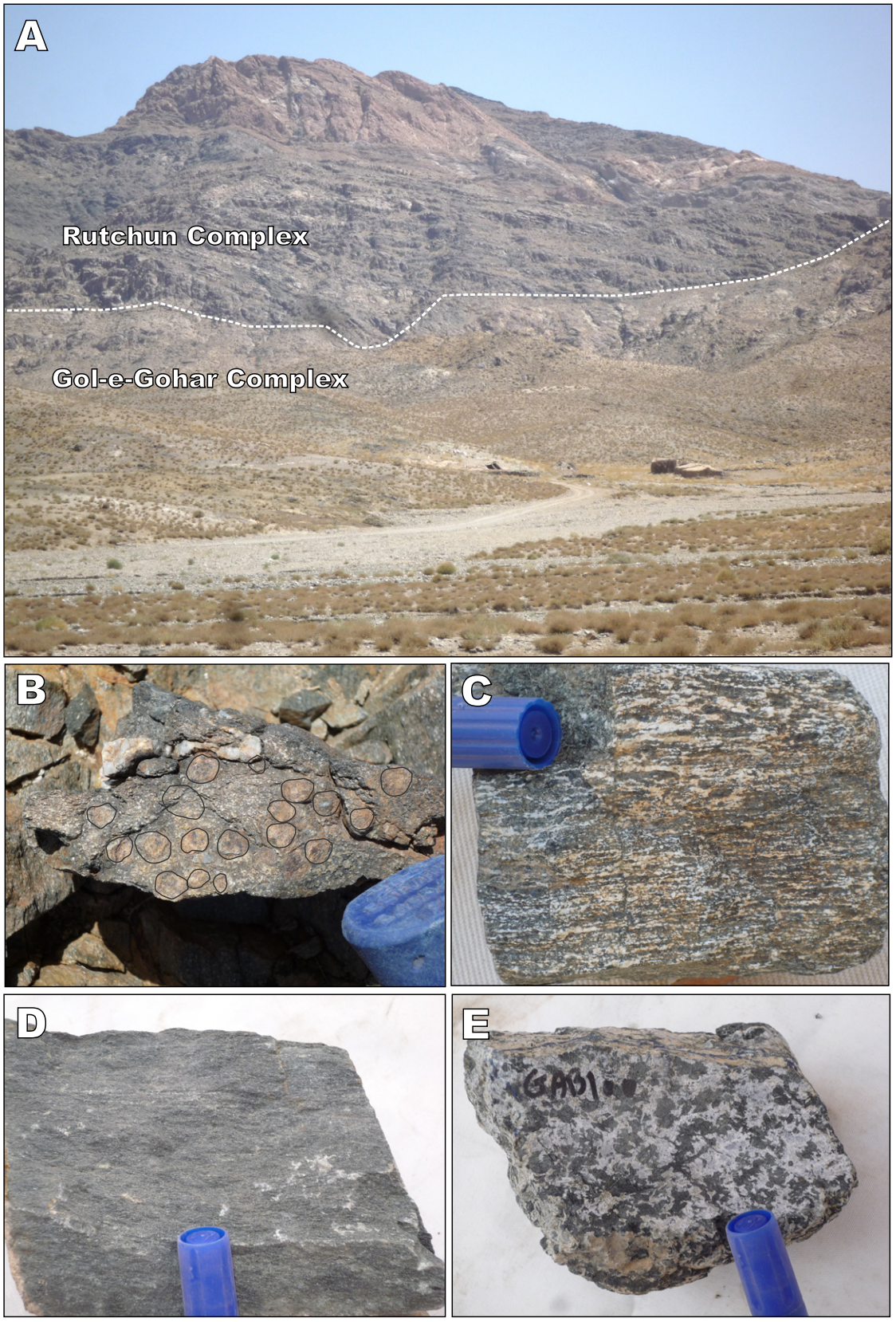

FIGURE 2. Field characteristics of Gol-e-Gohar Complex in the study area. A) Panoramic view of Gol-e-Gohar metamorphic Complex overlain by the Rutchun Complex. B) Coars-grained garnets in metabasite. C) Ribbon-textured garnet-free metabasites occurred as dark amphibole-rich and light plagioclase-rich bands. D) Garnet-free metabasites with amphibole porphyroblasts (up to 70vol.%). E) Coarse grained dark colored amphibole and the white colored feldspars in metagabbro.

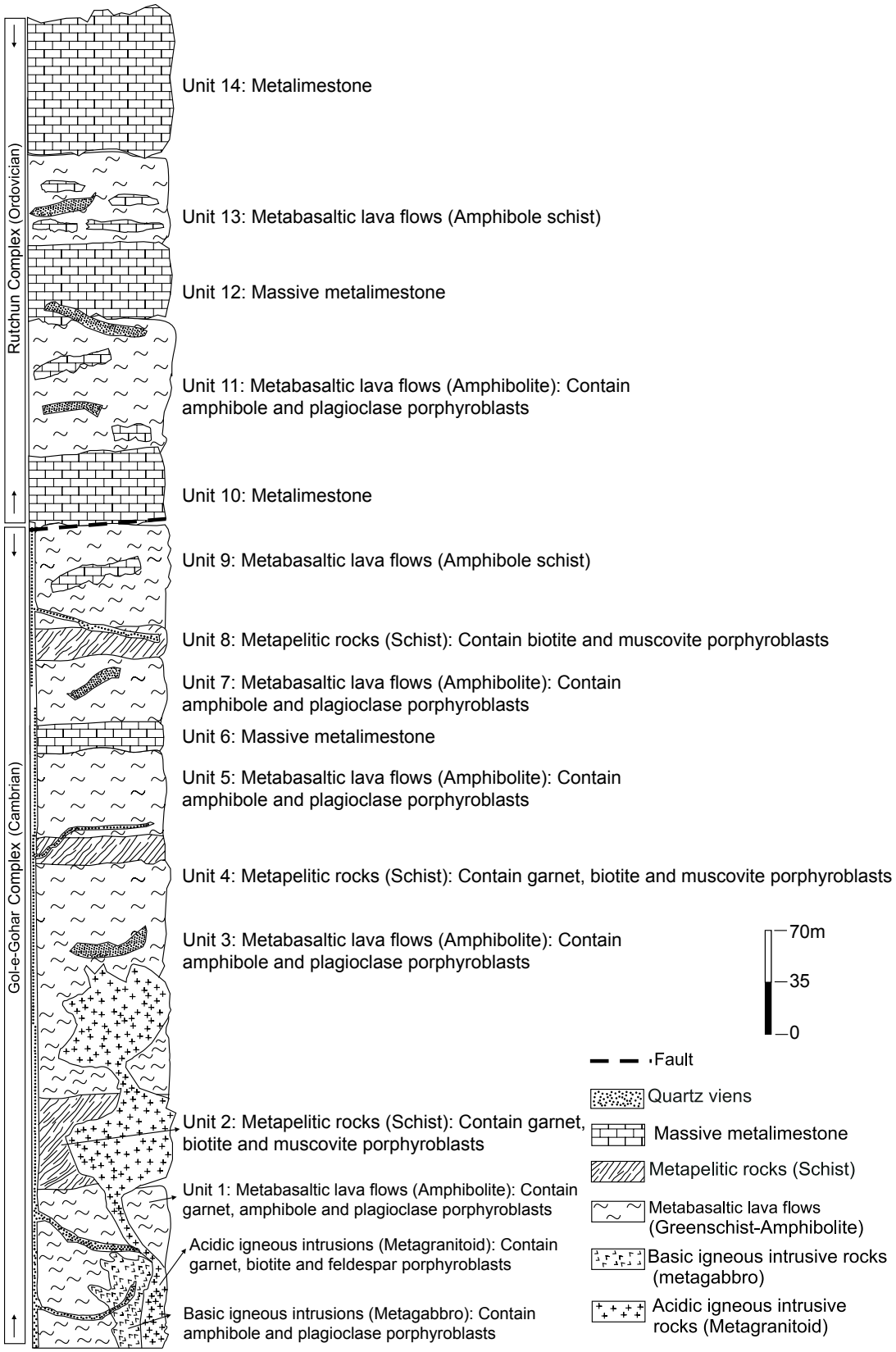

FIGURE 3. Measured stratigraphic column of Gol-e-Gohar metamorphic Complex in the western part of the study area. See Figure 1 for location.

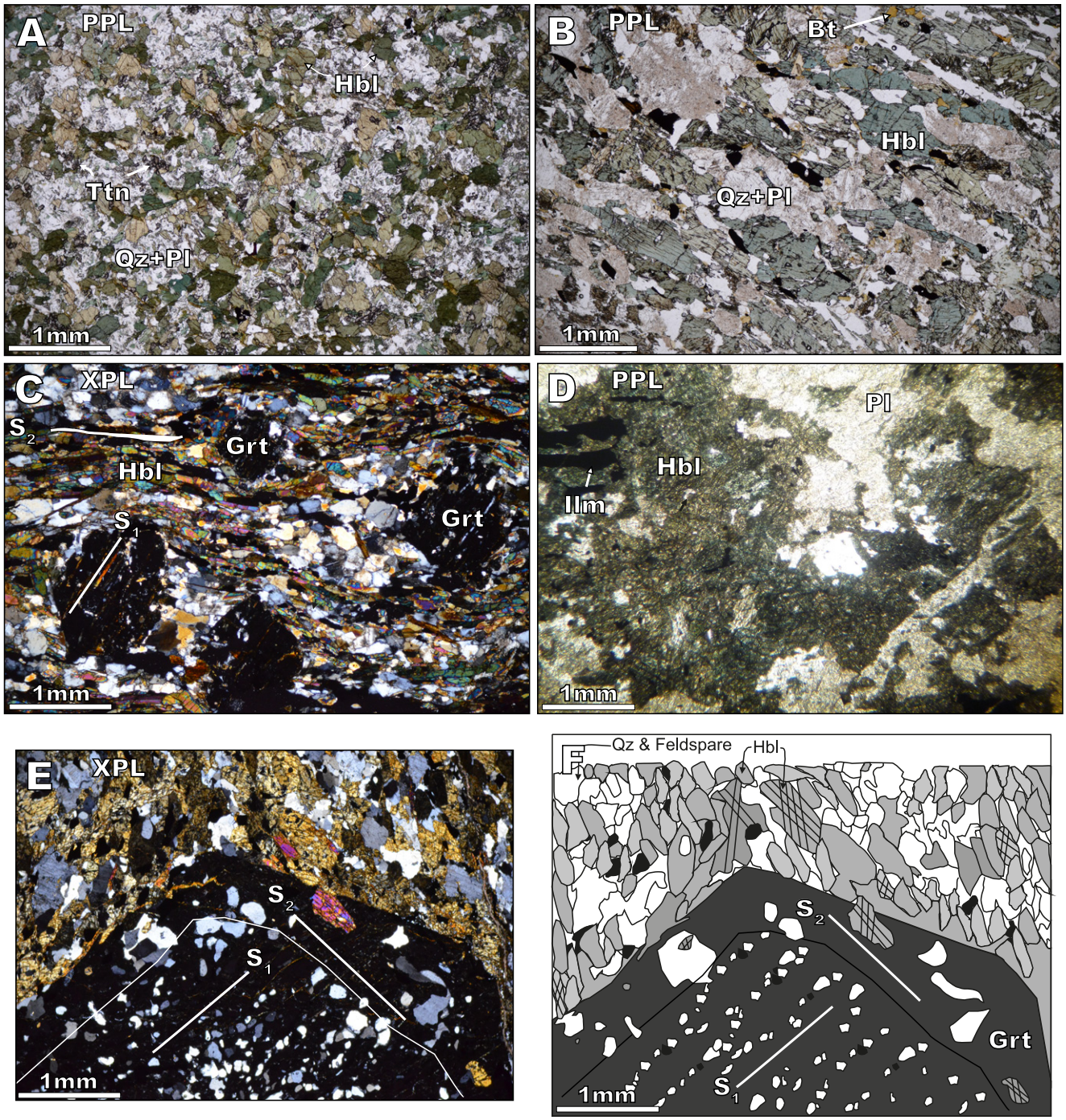

FIGURE 4. Photomicrographs of Gol-e-Gohar metamorphic Complex. A) Low-grade metabasites with epidote, chlorite and actinolite-hornblende along with sericite and calcite. B) Ribbon texture as dark amphibole-rich and light plagioclase-rich bands in garnet-free metabasites. C) Hornblende, biotite, and plagioclase in garnet-bearing metabasites. These minerals have oriented parallel to the main foliation and garnets have grown on the S_1 foliation. D) Coarse-grained hornblende and plagioclase with granoblastic texture in metamorphosed gabbros. E) Large garnet porphyroblast with two growth stages. F) Schematic illustration of Figure 4E. Abbreviations of mineral names are from Whitney and Evans (2010). Abbreviations: Hbl: Hornblende; Pl: Plagioclase; Qz: Quartz; Grt: Garnet; Ilm: Ilmenite; Ttn: Titanite (sphene); Cross-Polarized Light (XPL) and Plane-Polarized Light (PPL).

and 45% plagioclase with banded and granoblastic textures (Fig. 4D). Hornblende porphyroblasts with an aspect ratio of ~2:1 to 6:1 and up to 20mm in length are oriented in the direction of the main foliation (S_2). Petrographically, there are two shapes of biotites in these rocks. Coarse-grained biotites (with maximum 6mm in length, and aspect ratios of ~2:1 to ~4:1) which have developed parallel to the hornblendes and S_2 foliation, so they are syn-tectonics. The

second shape are those biotite crystals which have been grown on the second foliation (S_2), and seen as randomly oriented crystals.

They can be interpreted as post tectonic phases Two types of garnet have been identified in these rocks. Type 1are pale-brown isotropic hypidiomorphic to hexagonal porphyroblasts which contain oriented inclusion trails of quartz, biotite, and plagioclase. Inclusion trails have distributed throughout the crystals and make an angle of 50°–70° with external S_2 foliation. Therefore, the dominant foliation in these rocks is not parallel with the orientation of inclusion trails in the garnets. These garnet porphyroblasts have euhedral shapes and show smooth boundaries without any strain caps, strain shadows and deformation features, therefore, they are post tectonics and have grown on the first foliation (S_1) (Fig. 4C). The second Type of garnets characterised by two parts. In the central part, they contain oriented inclusion trails of quartz, feldspar, and opaque minerals which have been persisted from S_1 foliation. Inclusion trails developed more or less perpendicular to the S_2 foliation. It seems that the central parts of these garnets developed after S_1 foliation and then, during the second deformation phase (D_2), S_2 foliation developed and the marginal parts crystallized as overgrowth margins of the garnet cores. Marginal parts of these porphyroblasts have some inclusions trails parallel to the surrounding foliation (Fig. 4E, F).

The marginal parts of garnets show smooth-surfaces without any strain caps or strain shadows moreover, hornblende porphyroblasts (belont to the S_2) have been penetrated into their rims. Inclusion trails within the rims are parallel to the rock dominant foliation, suggesting that the outer parts of the garnets are post tectonic and crystallized on the S_2.

Mineral chemistry

Amphibole

The chemical composition of Gol-e-Gohar metabasites are reported in Table 2. Separation of Fe^{2+} and Fe^{3+} in structures of the amphiboles was conducted using Droop (1987) stoichiometric method (Table 2). According to their chemical composition, $((Ca+Na_B)\geq 1;\ Na_B<0.5;\ Ca>1.5)$ atoms per formula unit (apfu) (Leake *et al.*, 1997), the amphiboles belong to the calcic series and are tschermakite and ferro-tschermakite (Fig. 5A) (nomenclature from Leake *et al.*, 1997).

In the Al^{IV} *vs.* Sum-A+Al^{VI}+Fe^{3+}+2Ti diagram (Fig. 5B; Pe-Piper, 1988), amphibole data show a straight linear relationship coincident with the tschermak substitution trend. Moreover, the Na_A/Al^{IV} and Al^{VI}/Al^{IV} ratios in the amphiboles are 0.125 and 0.525, respectively, which also suggest a tschermak substitution.

Garnet

Electron microprobe analyses of garnets (Table 3) have been done from the central part to the rim in the samples GB-93 and GB-259, and separation of Fe^{3+} from Fe^{2+} have been done using Droop (1987) equation (Table 3). In the sample GB-259, garnets show a single growth stage after S_1 (Fig. 4C), but in the sample GB-93, they show two growth stages (Fig. 4E, F). The MgO average concentration in the sample GB-93 and in post S_2 garnet rims, is 3.18%. This value is slightly higher than in post S_1 parts of the garnets (Table 3). In the central part of the post S_1 garnets from the samples GB-259 and GB-93, X_{prp} and X_{Fe}(Fe/(Fe+Mg)) values are almost similar in two samples, but, in the rims, X_{prp} value increases and X_{Fe} decreases relative to the cores. In combinational profiles (Fig. 6), the pyrope

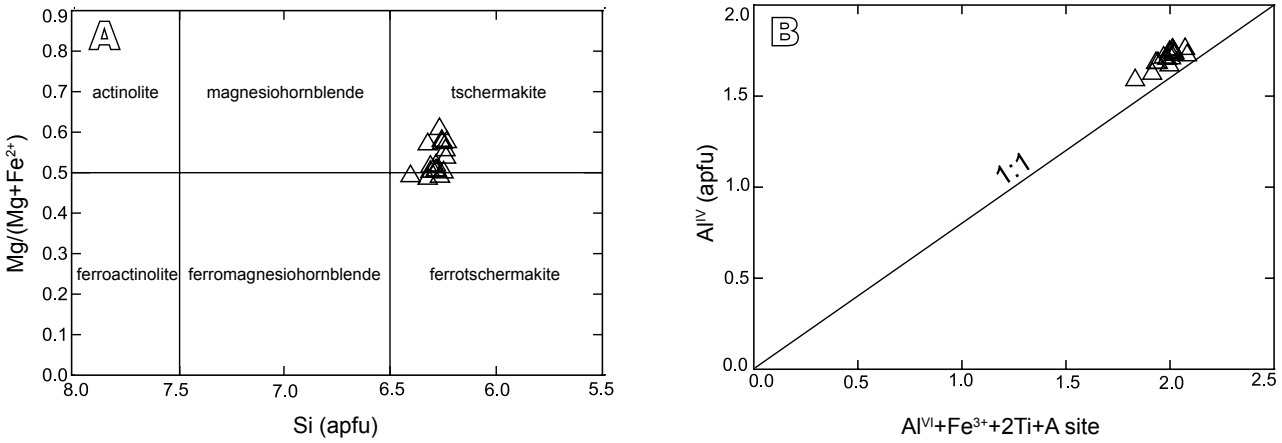

FIGURE 5. A) Chemical composition of amphiboles from Gol-e-Gohar metabasites. Nomenclature from Leake *et al.* (1997). Amphibole formula calculated following Holland and Blundy (1994). B) In the Al^{IV} *vs.* Sum-A+Al^{VI}+Fe^{3+}+2Ti plot (Pe-Piper, 1988), amphiboles show straight linear relationship.

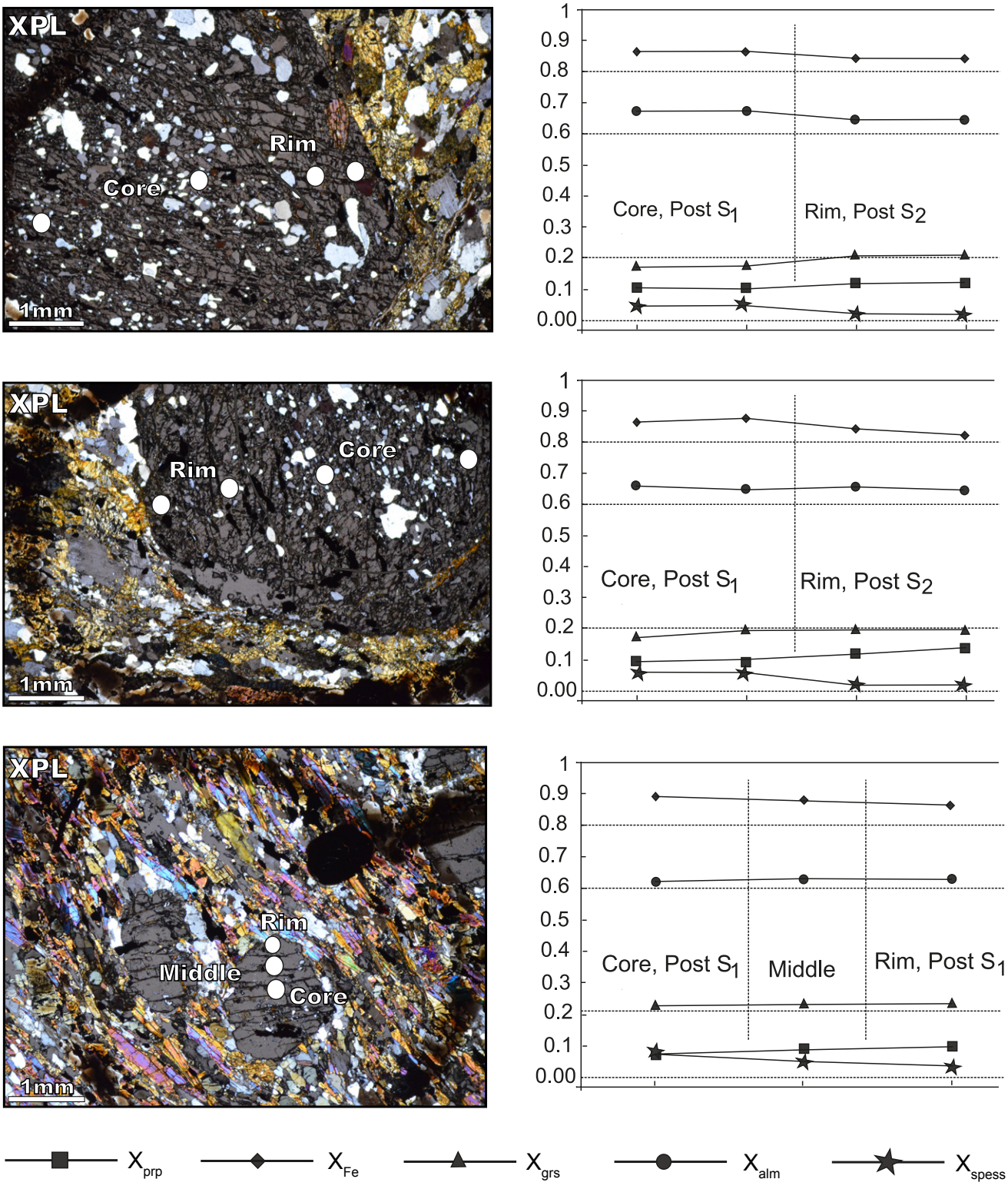

FIGURE 6. Chemical variations from the center to the rim in the garnets, X_{alm}, X_{Fe} and X_{spess} decrease and pyrope content increases. Abbreviations: Xalm: almandine proportion, X_{prp}: pyrope proportion, X_{grs}: grossular proportion, X_{spess}: spessartine proportion, X_{Fe}: $Fe/(Fe+Mg^{2+})$, Cross-Polarized Light (XPL), S_1: Schistosity, S_2: Schistosity.

content increases from the center to the rim, but X_{alm}, X_{Fe}, and X_{spess} decrease.

Plagioclase

The average values of Ab, An and Or in the plagioclase are: Ab (75.83), An (26.346) and Or (0.752) (Table 4). The An component slightly increases from the center to the rim (about 2%), suggesting the effect of pressure and temperature during progressive metamorphism in the metabasites (Kapp *et al*., 2009). Small values of An in the plagioclases along with small-values of CaO (~4.98wt.% on average) *versus* higher-amounts of Na_2O (8.9wt.%) are in acordance with the effect of pressure during crystallization.

Biotite

The chemical composition of biotites from the metabasites is shown in Table 5. The average value of MgO is 12.01wt.% and of TiO_2 1.54wt.%. The relatively high $Mg/(Mg+Fe^{2+})$ ratio, TiO_2 value, and presence of minerals such as sphene, magnetite, ilmenite, and quartz in the metabasites suggest high oxygen fugacity conditions during the crystallization of biotites (Árkai *et al*., 2002; Kapp *et al*., 2009).

Ilmenite

The chemical compositions of ilmenites in Gol-e-Gohar metabasites are shown in Table 5. These minerals characterised by high amounts of FeO and TiO_2 and small amounts of SiO_2, MgO and Al_2O_3 oxides. Ilmenite grains distribute among the amphibole andbiotite crystals and set in the matrix indicating that they have been formed due to diffusion of Ti between amphiboles, biotites and the matrix. The presence of ilmenite also indicates a moderate to high oxygen fugacity during crystallization of ilmenites in the metabasites (Wones and Eugster, 1965).

TABLE 7. Temperature and pressure calculations for Gol-e-Gohar metabasites

Complex	Gol-e-Gohar		
Rock Type	Metabasite		
Sample	GB-259	GB-93	GB-38
Thermometers			
Hbl-Pl (H and B, 1994)	630 – 660°C	640 – 680°C	620-670°C
Ti in Hbl (O, 1984)	630 – 650°C	640 – 660°C	610-660°C
Barometers (Al in Hbl)			
P(1) Kbar (H and Z, 1986)	8–9.5Kb	8–10Kb	7.8-10Kb
P(2) Kbar (H *et al.*, 1987)	9–10Kb	9–10.5Kb	7.5–9.5Kb
P(3) Kbar (J and R, 1989)	7–7.5Kb	7–8Kb	7.7–8.5Kb
P(4) Kbar (S, 1992)	8.7–9.5Kb	8.7–10.5Kb	8.5–10Kb
P(5) Kbar (A and S, 1995)	8.5–9.5kb	9–10Kb	8–10.5Kb

Abbreviation: (O, 1984):Otten, 1984; (H and B, 1994): Holland and Blundy, 1994; (H and Z, 1986): Hammarstrom and Zen, 1986; (H *et al.*, 1987): Hollister *et al.*, 1987; (J and R, 1989): Johnson and Rutherford, 1989; (S, 1992): Schmidt, 1992; (A and S, 1995): Anderson and Smith, 1995. P(1): P(±3kbar)=-3.92+5.03 Al(Total); P(2): P(±1kbar)=-4.76+5.64 Al(Total); P(3): P(0.5kbar)=-3.46+4.23 Al(Total), P(4): P(±0.6kbar) =-3.01+4.76 Al(Total), and P(5) [±0.6Kb]=(-3.01+4.76 AlTotal)–{(T-675)/85}{0.53 AlTotal +0.005924(T– 675)}.

Thermobarometry

In this work, to calculate the pressure and thermal conditions in the formation of metabasites, we used i) the hornblende-plagioclase thermometer (Holland and Blundy 1994); ii) temperature estimations based on Ti values in the hornblende structure (Otten, 1984) and iii) geobarometry based on Al values in hornblende (Schmidt, 1992) (Table 7).

Hornblende-plagioclase thermometer

The hornblende-plagioclase thermometer of Holland and Blundy (1994) is applicable in the P-T range 400–1000ºC and 1–15kbar on a broad range of bulk composition and is based on two reactions involving amphibole and plagioclase end members:

Edenite+Quartz=Tremolite+Albite (1)

Edenite+Albite=Richterite+Anortite (2)

Because reaction (2) is only applicable for quartz-absent hornblende-bearing assemblages, so, we use reaction (1) and consider a pressure of 10kbar for calculating the temperature conditions of the studied samples. The sensitivity of this thermometer to plagioclase contents is minimal. For calculating metamorphic conditions, we used chemical compositions of the cores and rims of both amphibole and plagioclase. Textural evidence such as straight boundaries between the hornblendes and plagioclases and the lack of replacement features between them (Fig. 4B) shows that they are in equilibrium. Also, in the case of use of the hornblende and plagioclase rim, due to probable retrograde effects of values very near the edge has been avoided. The calculation of peak M_2 metamorphic conditions using hornblende-plagioclase thermometer (Holland and Blundy, 1994) yield an average temperature of ~650–680ºC for the metabasites (Table 7). The calculated temperature for peak metamorphic condition is accordance with microscopic studies and mineral chemistry of the metabasites.

Ti values in the hornblende structure

Ti value in amphibole is independent of the amounts of the TiO_2 in the whole rock and is mainly dependent on the increase of metamorphic grade (Robinson *et al*.,

1982). In order to calculate the temperature in terms of Ti value in amphibole, we used experimental thermometer (Otten, 1984) that is as T(ºC)=1204*(Ti/23O)+545. The highest Ti content in hornblende has been used to calculate the M_2 metamorphic conditions. This thermometer indicates temperatures of about ~640–660ºC for the peak metamorphic conditions. The results of the multiple-equilibria calculations (Table 7) are in good agreement with those from the other methods.

Geobarometry based on Al value in hornblende structure

To calculate the pressure, we used the geobarometer from Schmidt (1992). Pressure was obtained from the following equation:

$$P[\pm 0.6Kbar] = -3.01 + 4.76Al_{Total} \quad (3)$$

This geobarometer indicates pressures between 7 and 10.5kbar for the formation of the amphiboles. Other results of pressure estimations for the studied rocks are listed in the Table 7.

Geochemistry

Whole rock composition

Whole rock chemical composition of metabasites is in Table 1. TiO_2 is between 1.32 to 3.40, with a mean value of ~2.16wt.%. This oxide is mainly concentrated in minerals such as ilmenite and sphene. Mg# values (Mg#=100*molar $MgO/(MgO+FeO_T)$) in garnet-bearing metabasites are between 0.33 and 0.45, but in garnet-free metabasites are slightly higher and varies between 0.40 and 0.51. Based on the chemical composition, the parent rocks of these metabasites are basalts with a tholeiitic signature (Fig. 7A, B).

With increasing SiO_2, a decrease in MgO, CaO, Ni and La, and an increase in K_2O, TiO_2, Na_2O, Rb, and Ba are observed (Fig. 8). With increasing Zr, the oxides FeO_T and TiO_2 increase and MgO decreases (Fig. 8). Moreover, as indicate in Zr *vs*. TiO_2 and Zr *vs*. FeO_T diagrams (Fig. 8), TiO_2 values have been increased and Mg# decreased during also in Mg# *vs*. TiO_2 diagram (Fig. 9) magma differentiation in the parent magmas.

Trace element and REE geochemistry

In the primitive mantle-normalized element concentration diagram (Fig. 10A), Large Ion Lithophile Elements (LILE) and High Field Strength Elements (HFSE) have been enriched up to 100 and 10 times with respect to the primitive mantle, respectively. Moreover, in the studied rocks, LILE slightly enriched relative to the HFSE and samples, show some what enrichment of K, Rb, Ba, Cs, Th, Nb, and Ce are observed (Fig. 10A).

In the the Mid Ocean Ridge Basalt (MORB)-normalized element concentration diagram (Fig. 10B), HFSE values are similar to those in the MORB, and the LILE contents enriched up to 70 times relative to the MORBs, and in this way, they are compared with intra-continental plate basalts (Pearce, 1983), wherease, in the Enriched-MORB (E-MORB)-normalized element concentration diagram (Fig. 10C), the HFSE contents in the metabasites are very similar to those in the E-MORBs except only small enrichments in LILE contents of the studied metabasites. Besides, a slight enrichment in Light REE (LREE) (La/Yb_N=2.68-7.61) is also observed (Fig. 10D). Parallel REE patterns in the metabasites (Fig. 10D), show that the parent magmas probably have more or less common sources and suggest that crystal fractionation may not had an important role in the formation of these rocks. Depletion of HREE or HFSE in the chemical compositions of metabasites, is not observed.

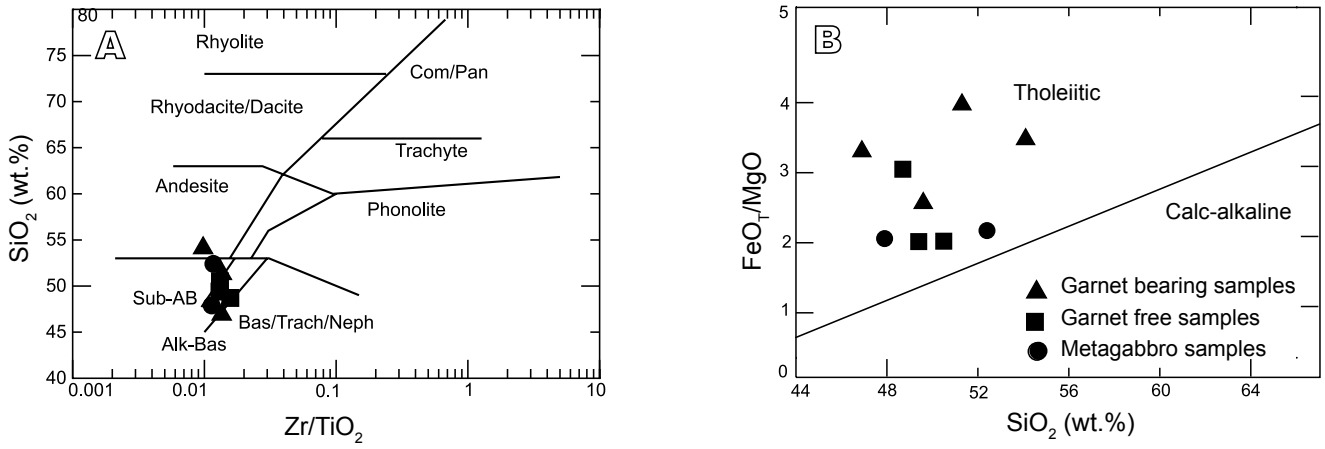

FIGURE 7. A) Chemical compositions of metabasites in a Zr/TiO_2 *vs.* SiO_2 diagram (Winchester and Floyd, 1977), their parent rocks are tholeiitic basalts. B) Chemical compositions of metabasites in a SiO_2 *vs.* FeO_T/MgO diagram (Rickwood, 1989).

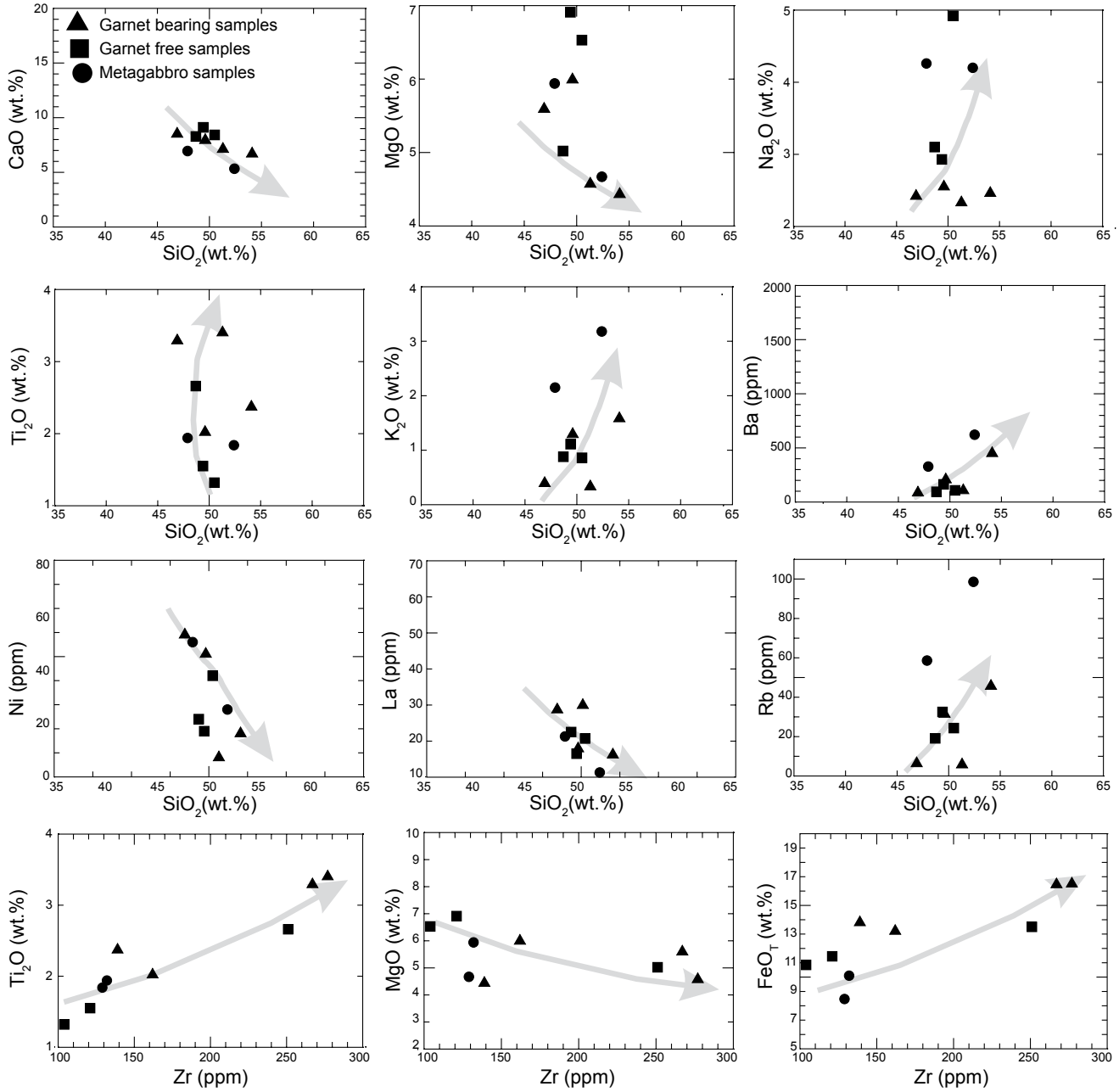

FIGURE 8. Major oxides and trace element abundance *vs.* SiO_2 (wt.%) and Zr (ppm) in metabasites.

Sr-Nd isotope geochemistry

Sr and Nd isotopic analysis were performed on 4 whole rock samples and the values were calculated according to the age of 550Ma (Cambrian, the age of the Gol-e-Gohar Complex (Sabzehei *et al.*, 1997) (Table 6). In the Gol-e-Gohar metabasites, the initial $^{143}Nd/^{144}Nd$ ratios vary between 0.511913 to 0.512067 and εNd^{550Ma} values are -0.31 to 2.68. Initial $^{87}Sr/^{86}Sr$ ratios vary from 0.708236 to 0.709791 and εSr values are 62.29 to 84.38, but for sample GB-103, initial $^{87}Sr/^{86}Sr$ ratio and εSr value are 0.715088 and 159.64, respectively (Fig. 11A, B). As shown in Figure 11A and B, the studied samples plot in the mantle array field. Concentration of the data in the right-down part of the diagram may suggest that their source have been enriched from incompatible elements before partial melting.

Initial $^{87}Sr/^{86}Sr$ ratios (0.708236 to 0.709791) in three samples, GB-38, GB-93 and GB-259, also show mantle source enrichment (the source may be sub-continental lithospheric mantle) (Fig. 11C), but in sample GB-103, initial $^{87}Sr/^{86}Sr$ ratio (0.715088) is higher. This increase may be due to effect of sea water, high Rb/Sr ratios in the mantle source and/or crustal contamination (Verma, 2009).

In the $^{87}Sr/^{86}Sr$ *vs.* Ba/Yb diagram (Fig. 11D), the studied samples show probable enrichment for the mantle sources.

DISCUSSION

Tectonic relationships and metamorphic conditions

Stratigraphical, structural and petrofabric studies in the study area show that three metamorphic events and four deformation phases have affected the rock units. In metabasites with middle to lower greenschist facies, the formation of unoriented chlorite, epidote, actinolite, hornblende, and opaque minerals are associated with the first deformation phase (D_1). The second metamorphic event (M_2) acted simultaneously with the second deformation phase (D_2). The S_2 foliation in the metabasites appears as dark amphibole-rich and light plagioclase-rich bands (Fig. 4B, C). The third metamorphic event (M_3) formed during the third deformation phase (D_3) and produced fine muscovites parallel to the shear zones. Also in this stage, the rocks were affected by retrograde metamorphism and mylonitic structures developed (local S_3 foliation). In the fourth deformation phase (D_4) the rock units were faulted and disrupted. The main metamorphism and deformation processes in the Gol-e-Gohar units were coincident with the early Cimmerian orogenic phase. Minerals such as sphene, magnetite, ilmenite and quartz associated with amphibole and biotite in the metabasites, indicate high oxygen fugacity conditions during crystallization of amphiboles and biotites. High oxygen fugacity during the crystallization of biotites can cause great amounts of Mg and Ti enter into the biotite structure (Kapp *et al.*, 2009). On the other hand, low An and CaO content in plagioclase correlates with pressure effect during crystallization (Kapp *et al.*, 2009). According to the mineral composition, a temperature of ~650–680ºC and pressures between 7 and 10.5kbar are estimated for the matebasites. Moreover, thermobarometric estimations show that the peak of metamorphism occurred under medium- to high-temperature and medium-pressure conditions which is typically a characteristic of the metamorphic evolution of orogenic belts whose formation involved tectonic thickening of the crust (Kryza and Pin, 2002).

Petrogenesis

Fractional crystallization

Geochemical data and clear trends in the graphs in Figure 8 indicate that the fractionation trends observed in the parental magma of metabasites may be related to fractionation of olivine and pyroxene. Plagioclase fractional crystallization may have not occurred as suggested by the lack of negative Eu anomalies in the chonderite-normalised REE pattern (Fig. 10D). As seen in the Zr *vs.* TiO_2 (Fig. 8) and Mg# *vs.* TiO_2 diagrams (Fig. 9), the parent magmas of metabasites have undergone little differentiation. Moreover, this characterictic, which is commonly observed in tholeiitic magmas, indicates that neither Fe- and Ti-rich oxides nor Ti-rich hornblendes have separated during differentiation. It seems that the parental magmas of the metabasites had the same origin. Besides, different tectonic and magmatic events in the rift system and the replication of extensional phases over time could affect the type of magma generated.

Crustal contamination

The HFSE negative anomalies are a main feature of continental rocks and attributed to participation of the crust in the magmatic processes (Nagudi *et al.*, 2003). Since, these metabasites derived from the mantle, the lack of HFSE anomalies in their composition suggests they have not been affected by crustal contamination and/or its effect is negligible. Therefore, Nb-Ta anomalies are very important to interpret the tectonic setting of basalts, because they show the effects of subducted slab or crustal contamination in the compositions of magmas (Gower and Swinden, 1991). So, whether this partial Nb-Ta enrichment, along with the little enrichment in K, Ba, Rb, and Th, in the Gol-e-Gohar metabasites, are in connection with crustal contamination of the parent magmas or related to their origin is still not clear. The Nb anomaly parameter (Nb/Nb*) (Verma, 2009) proposed to interpret the tectonic setting is:

$$(Nb/Nb^*)_{pm}=2(N_{bsa}/Nb_{pm})/(B_{asa}/B_{apm})+(L_{asa}/L_{apm}) \quad (4)$$

This parameter $(Nb/Nb^*)_{pm}$ for the metabasites shows values between 0.2 and 1.75, ~0.9 on average. Back-arc, rifting, and extensional basalts with negative Nb anomalies

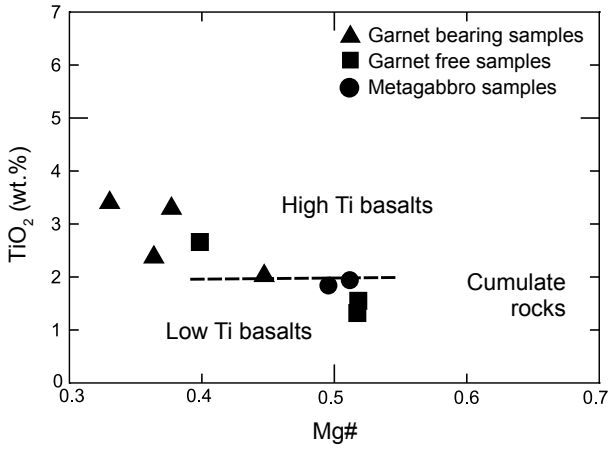

FIGURE 9. Mg# *vs.* TiO_2 diagram. Notice the negative relationship between Mg# and TiO_2 in the metabasites.

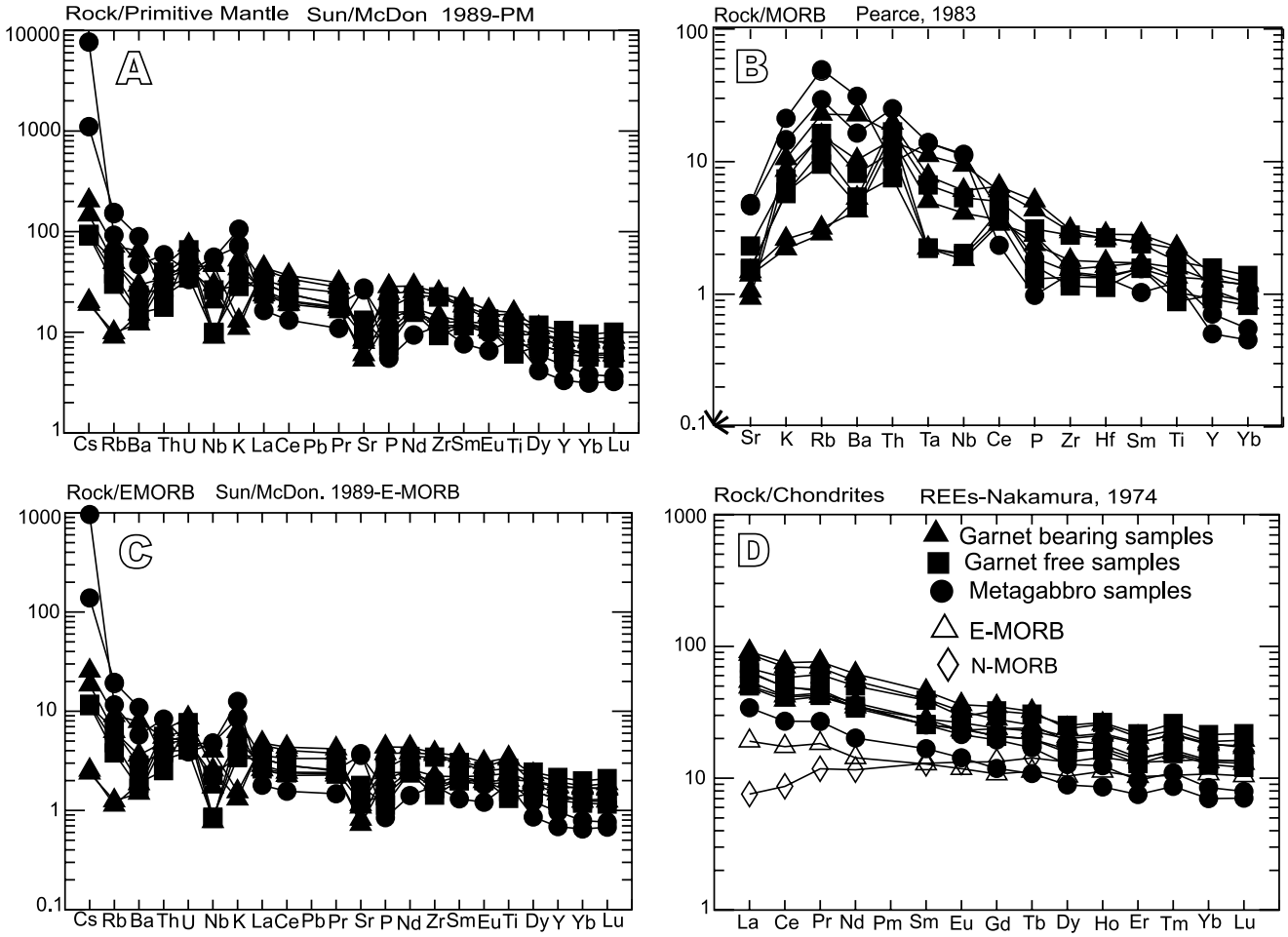

FIGURE 10. A) Primitive mantle-normalized patterns (Sun and McDonough, 1989) for Gol-e-Gohar metabasites. B) N-MORB-normalized patterns (Sun and McDonough, 1989) of trace elements from the studied metabasites. C) E-MORB-normalized patterns (Pearce, 1983) of metabasites. D) Parallel REE patterns in chondrite-normalized REE abundance in the metabasites (Nakamura, 1974). Composition of E-MORB and N-MORB according to Sun and McDonough (1989). N-MORB: Normal-Mid Ocean Ridge Basalt, E-MORB: Enriched-Mid Ocean Ridge Basalt.

show values of $\{Nb/Nb^*\}_{pm}>1$, whereas values of $\{Nb/Nb^*\}_{pm}$ between 0.37 and 0.85 with negative Nb anomaly are related to intra-continental rifting, continental break-up, and intra-continental extensional basalts (Verma, 2009).

The Gol-e-Gohar metabasites, that lack negative Nb anomalies and have $\{Nb/Nb^*\}_{pm}$ values of ~1, may have not been largely affected by crustal contamination. Indeed, LILE enrichment of the studied rocks in the MORB-normalized multi-element diagram probably is related to their within-plate enriched mantle sources (*e.g.* sub-continental lithospheric mantle) and this chemical feature can be formed due to small degrees of partial melting of the source.

Crustal contaminated basic igneous rocks are characterize by having ratios of La/Ta>22 and La/Nb>1.5 (Hart *et al.*, 1989). In the majority of Gol-e-Gohar samples, these parameters are lower (La/Ta~4.52 to 21.50 and La/Nb~1.3), except for 3 samples (GB-38, GB-104 and GB-120). This features along with small ratios of Ce/Y=0.89–4.14 and Zr/Y=3.5–8.5, small SiO_2 content (45 to 54.10), high Mg# values (0.33 to 0.56), and lack of depletion in HREE and HFSE suggest that the parent magmas of metabasites have not been affected by crustal contamination or its effect is negligible.

Possible source of metabasites

The ratios of less mobile trace elements such as Th and Yb are independent of mineral sources, degree of partial melting and fractional crystallization, which means that their ratios reflect their ratios in the mantle source. In the Ta/Yb *vs.* Th/Yb diagram (Fig. 12A; Pearce, 1983), Th/Yb and Ta/Yb ratios reflect clear variations in the chemical composition of the mantle source (Aldanmaz *et al.*, 2000, 2006; Rolland *et al.*, 2000). In this diagram, data from the studied metabasites fall in the enriched mantle-

derived melt field just parallel to the trend of within-plate enrichment (W trend). In the Zr/Y *vs*. Nb/Y (Fig. 12B; Fitton *et al*., 1997) diagram, Nb/Yb *vs*. TiO_2/Yb (Fig. 12C; Pearce, 2008) diagram, and Nb/Yb *vs*. Nd/Yb (Fig. 12D; Pearce and Peate, 1995, Pearce *et al*., 1995) diagram, the enrichment in Zr, Nb, and Nd lead the samples to fall in the enriched mantle field. Ti/Y and Nb/Y ratios in within-plate basalts are higher than in other basalts. These differences indicate that the mantle source for these rocks is more enriched relative to the MORB and volcanic-arc basalt sources (Rollinson, 1996). High Ti/Y and Nb/Y ratios in the studied metabasites suggest an enriched mantle source for their primitive magmas. In addition, Sun and McDonough, (1989) believe that Zr/Y ratios higher than 2.46 and Zr/Nb ratios lower than 15.71 separate the enriched from the depleted sources of basalts. The Zr/Y ratio (3.68 to

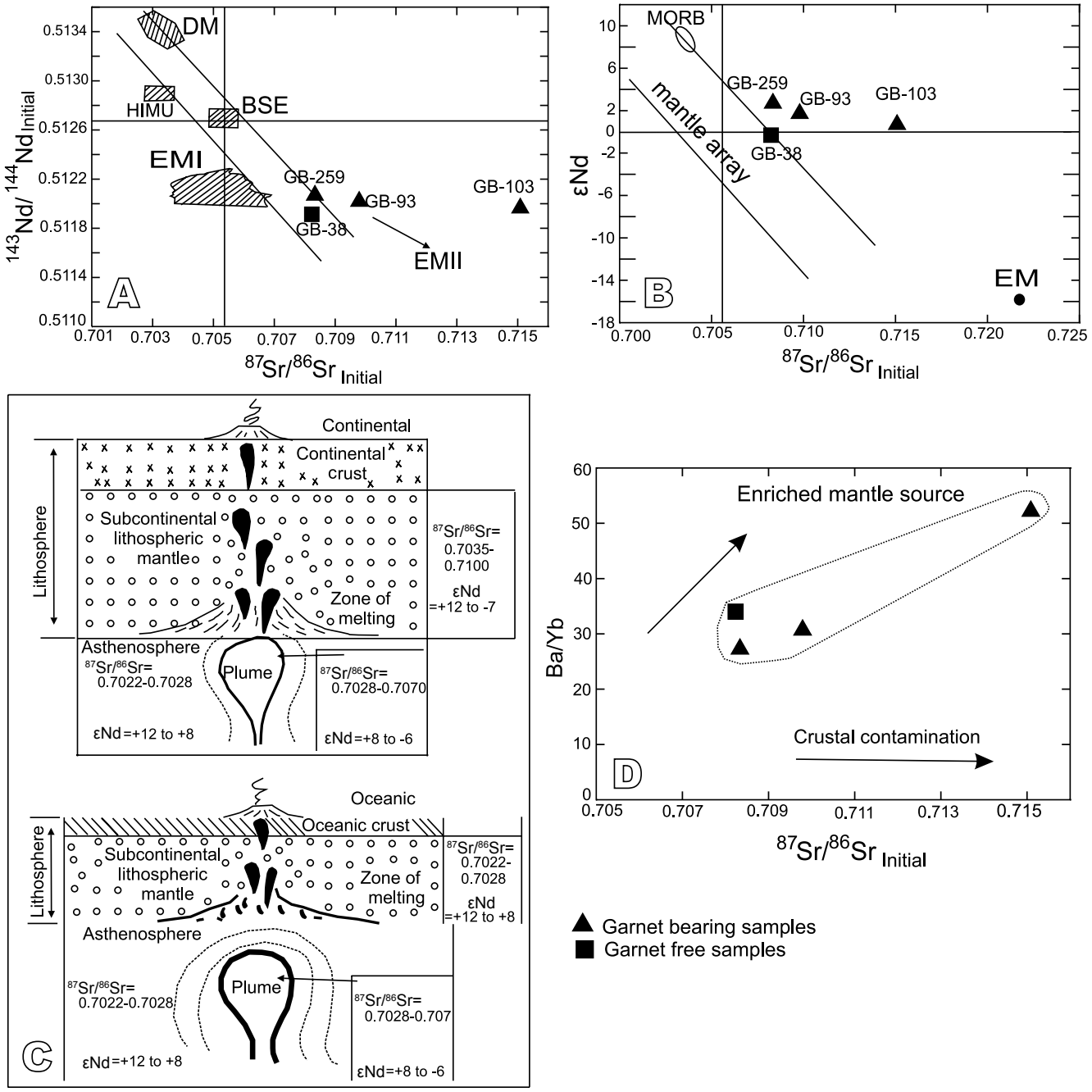

FIGURE 11. A) Initial $^{87}Sr/^{86}Sr$ *vs*. initial $^{143}Nd/^{144}Nd$ diagram. B) εNd values *vs*. initial $^{87}Sr/^{86}Sr$ diagram. In A and B, the studied samples plot on the lower right quadrant. C) Comparison between Sr and Nd isotopic ratios in active continental rift basalts and oceanic island basalts (McDonough *et al*., 1985). D) In the diagram of initial $^{87}Sr/^{86}Sr$ *vs*. Ba/Yb, the sources of Gol-e-Gohar metabasites show an enrichment trend. Abbreviations: DM: Depleted Mantle, EM: Enriched Mantle, HIMU: A source with a High $^{238}U/^{204}Pb$, BSE: Bulk Silicate Earth according to Zindler and Hart (1986).

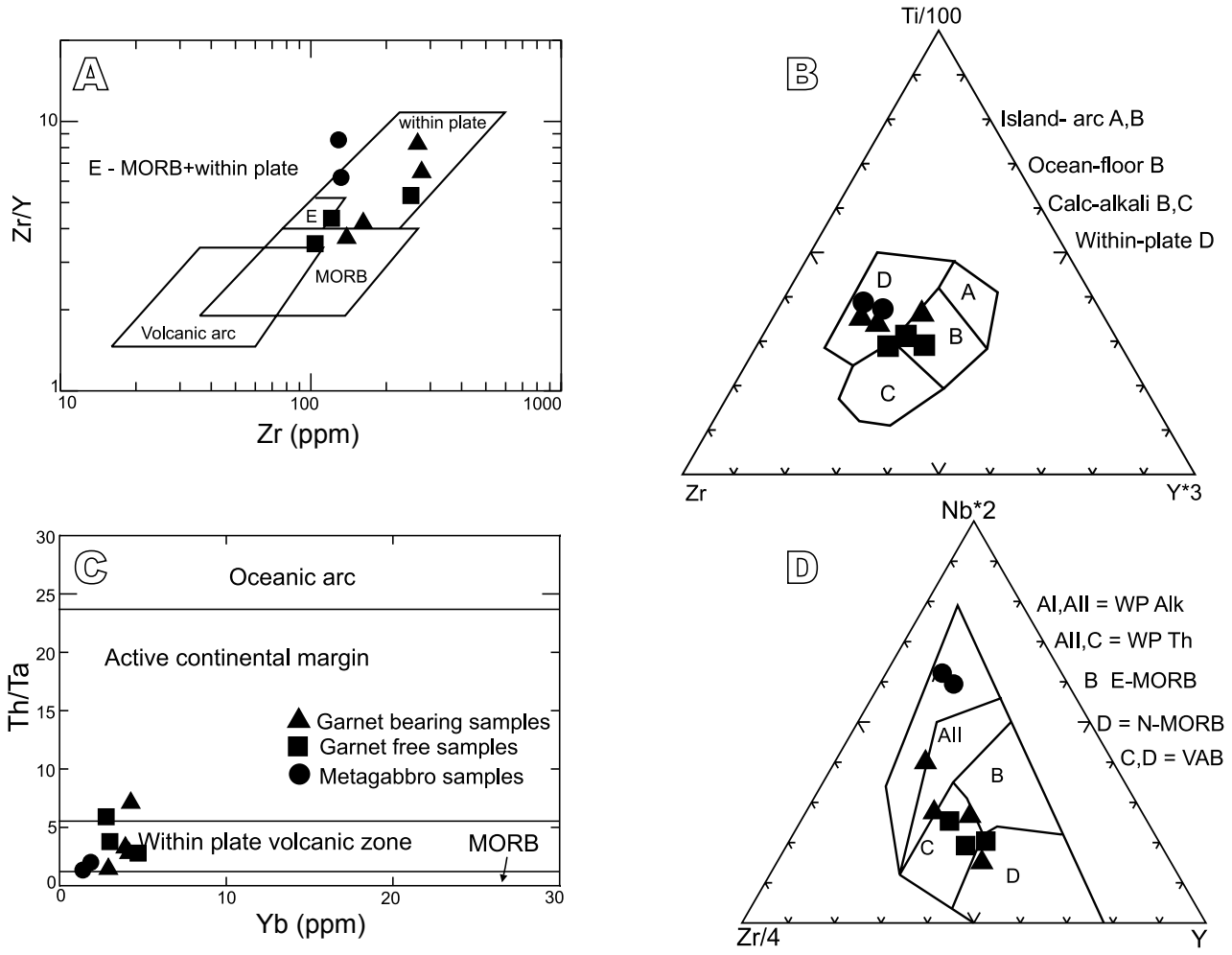

FIGURE 12. Trace element discrimination diagrams for Gol-e-Gohar metabasites. A) Zr *vs.* Zr/Y (Pearce and Norry, 1979). B) Ti, Y, and Zr (Pearce and Cann, 1973). C) Yb *vs.* Th/Ta (Schandl and Gorton, 2002). A–C) The metabasites fall in the within-plate environment. D) In the Zr, Nb, and Y triangular diagram (Meschede, 1986), metamorphosed gabbro samples trend toward continental within-plate alkali basalts, but the other Gol-e-Gohar metabasites (meta lava flows) show intra-continental tholeiitic affinity. Abbreviation: E-MORB: Enriched–Mid Ocean Ridge Basalt, N-MORB: Normal-Mid Ocean Ridge Basalt, VAB: Volcanic Arc Basalt, WP Alk: Within-Plate Alkaline, WP Th: Within-Plate Tholeiite.

8.54) and Zr/Nb ratio (1.5 to 21.71 with an mean value of ~9.66) in the samples indicate that they derived from an enriched mantle source. In Figure 12E, the Zr *vs.* Y diagram (Widdowson *et al.*, 2000) is used to evaluate the enrichment of source region. Accordingly, the metabasites are located in the enriched field.

Chondrite-normalized HREE abundances define the presence or absence of residual garnet in the source region (Jung, 2000). Because garnet retains the mantle HREE during partial melting, values of Yb_N more that 10 in the rocks suggest the lack of garnet as a residual phase in the source region (Wilson, 1989; Oliveros *et al.*, 2007). The Yb_N values of the metabasites are between 7 and 21.4 (14.27 on average), indicating of absence of garnet in the mantle source. In Sm/Yb *vs.* Ce/Sm diagram (Fig. 12F; Coban, 2007), metabasites from the studied area plot in the garnet-free lherzolitic mantle field. Besides, the presence of garnet in the mantle source, increases the Sm/Yb ratio in the melt, so, in Figure 12F, the Sm/Yb ratios for the metabasites are less than 2.5 indicating absence of garnet in their source. The average of $(Ce/Yb)_N$ ratio in the Gol-e-Gohar metabasites is ~4.75. According to Frey (1982), $2<(Ce/Yb)_N<5$ is characteristic of those magmas which have been formed in the range of spinel stability. In addition, when garnet persists as a residual phase in the source region, enrichment of MREE (such as Dy) relative to HREE (such as Yb) occurs. Because the Yb is preferentially accepted in the garnet structure (Peters *et al.*, 2008), average $(Dy/Yb)_N$ ratio in the studied metabasites is ~1.2, and this value indicates that garnet

does not play an important role in their source region (Lucassen *et al.*, 2008). In $(La/Sm)_{pm}$ *vs.* $(Tb/Yb)_{pm}$ diagram (Khudoley *et al.*, 2013; Will *et al.*, 2014; Fig. 12G), the metabasites fall in the spinel peridotite field too. Evidences such as the lack of garnet in the source region, the depths of spinel and garnet stabilities (Frey *et al.*, 1991) along with the Ce *vs.* Ce/Yb diagram (Fig. 12H; Ellam and Cox, 1991), the parent magmas of the Gol-e-Gohar metabasites have been come from depths of less than 80km and pressures of 20 to 25kbar.

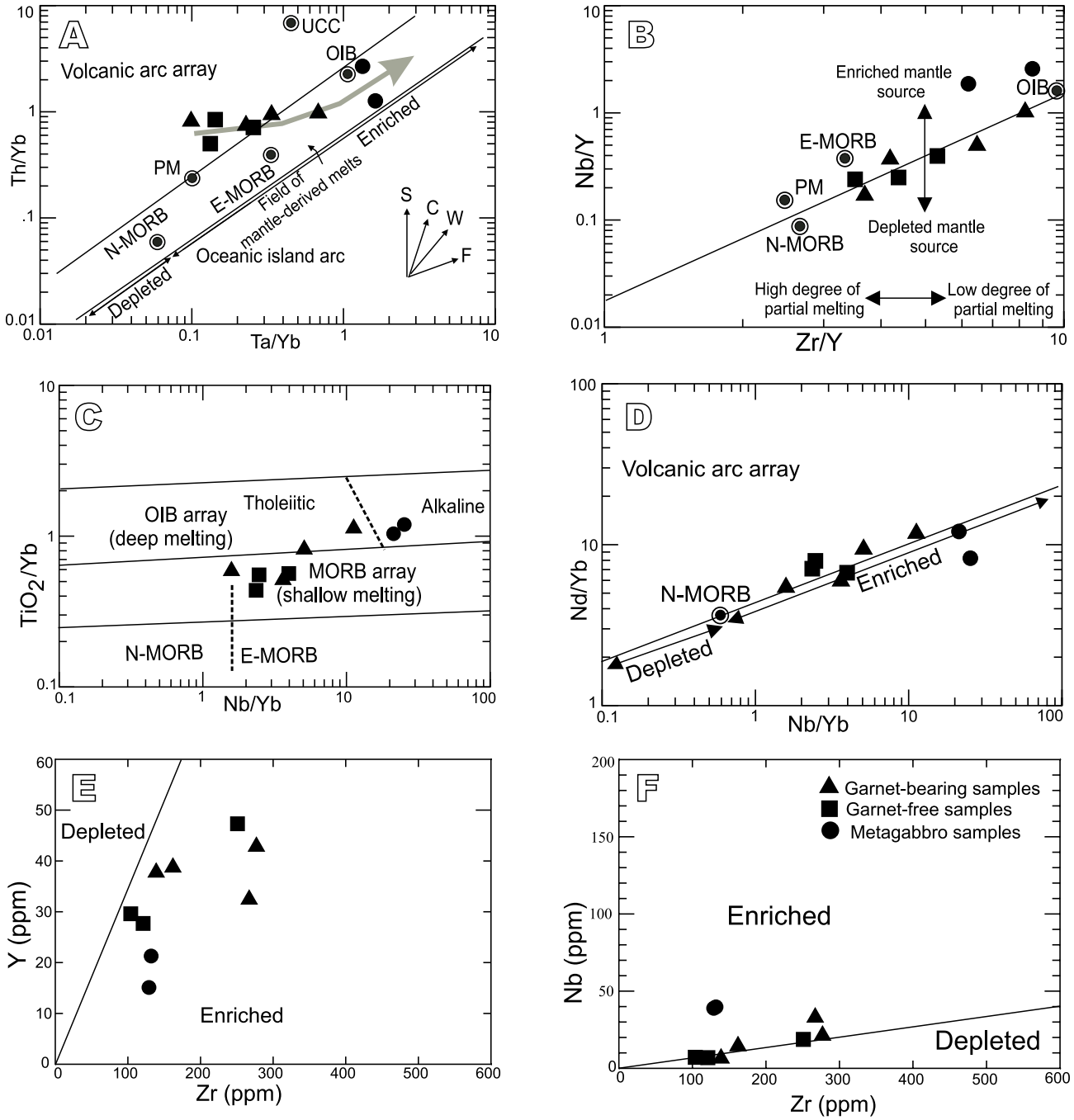

FIGURE 13. Discrimination diagrams for determination of the possible source of Gol-e-Gohar metabasites. A) Ta/Yb *vs.* Th/Yb (Pearce, 1983). B) Zr/Y *vs.* Nb/Y (Fitton *et al.*, 1997). C) Nb/Yb *vs.* TiO_2/Yb (Pearce, 2008). D) Nb/Yb *vs.* Nd/Yb (Pearce and Peate, 1995; Pearce *et al.*, 1995). E) Zr *vs.* Y. F) Sm/Yb *vs.* Ce/Sm diagram (Coban, 2007), the metabasites fall in the garnet-free lherzolitic mantle field. G) (La/Sm)pm *vs.* (Tb/Yb)pm diagram (Khudoley *et al.*, 2013; Will *et al.*, 2014), showing the spinel peridotite field for the metabasites. H) Ce *vs.* Ce/Yb diagram (Ellam and Cox, 1991), showing that the metabasites originated from depths of less than 80km and pressures between 20 and 25kbar. Composition of Enriched-Mid Ocean Ridge Basalt (E-MORB), Normal-Mid Ocean Ridge Basalt (N-MORB), Primitive Mantle (PM), Oceanic Island Basalts (OIB), Lower Continental Crust (LCC), and Upper Continental Crust (UCC) according to Taylor and MacLennan (1985) and Sun and McDonough (1989).

Tectonic setting

In Zr *vs*. Zr/Y (Fig. 13A; Pearce and Norry, 1979), Ti-Y-Zr (Fig. 13B; Pearce and Cann, 1973), and Yb *vs*. Th/Ta diagrams (Fig. 13C; Schandl and Gorton, 2002) the metabasites fall in the field of intra-continental basalts. Higher contents of Y and Zr, as well as high proportions of Zr/Y (between 3 to 8) (Pearce and Norry, 1979) represent a within-plate environment for the studied metabasites. In Zr-Nb-Y diagram (Fig. 13D; Meschede, 1986) these rocks show intra-continental rifting characters with tholeiitic to alkaline affinity. In this diagram, Gol-e-Gohar metamorphosed gabbroic intrusives tend to fall in the field of continental within-plate alkali basalts, but other metabasites (metamorphosed lava flows with layered structures) indicate intra-continental tholeiitic affinity.

Higher amounts of Nb/Y ratios in metamorphosed gabbros can be the cause of their alkaline signature. Crustal contamination decreases the Nb/Y ratio, so, high Nb/Y ratios (between 1.87 to 2.58) in the metamorphosed gabbros indicate that crustal contamination has not affected their parent magmas. Moreover, alkaline composition of these rocks suggest increasing thickness of the crust and decrease in degrees of partial melting (Wilson, 1989). On the other hand, evidences such as TiO_2 enrichments and high Zr/Y ratios (between 3 and 8) in the samples, reveal that they belong to an intra-continental rifting environment. Several authors propose that continental rifting, epeirogenic phases along with mafic magmatism and formation of numerous grabens occured in the Palaeozoic in the Iranian platform (Sheikholeslami *et al*., 2003).

Extensional processes of Iranian continental platform and ascending of underlying asthenosphere occurred in the Sanandaj-Sirjan metamorphic zone at Palaezoic era (Sheikholeslami *et al*., 2003). This conditions lead to the formation of vast depressions in which continental detritic sediments accumulated. At present, these sediments occur as different metamorphic complexes like the Gol-e-Gohar Complex in the Sanandaj-Sirjan metamorphic zone. Simultaneously, asthenosphere ascend and partially melted in spinel lherzolite stability field and then, tholeiitic primary magmas produced. The resulting melts became more enriched in LILE than the MORBs and probably, derrived from enriched upper mantle. The melts ascended toward the surface without significant crustal contamination and were emplace as lava flows between the sediments. The subsequent magmatic event in the area was the formation and emplacement of alkaline gabbro intrusions. Thereafter, in the early Cimmerian orogenic phase at the middle-late Triassic period (Mohajjel and Fergusson *et al*., 2003; Mohajjel and Fergusson, 2014), these sedimentary-igneous associations deformed and metamorphosed, and constitute the south-eastern Sanadaj-Sirjan metamorphic complexes. In this orogenic phase, the primary sediments changed into the slates, phyllites and schists, and the primary igneous rocks changed into the metabasites.

Tectonic implications

Geochemical dataset from the studied metabasites highlight an intra-continental rifting environment with tholeiitic to alkaline affinity. The Sr and Nd isotopic geochemistry, minor LREE and LILE enrichments and lack of high depletion in HREE reveal a garnet-free enriched mantel source, confirmed by $(Ce/Yb)_N$=3.65 in the metabasites. These features indicate that during the formation of the parent magmas, the thickness of the crust gradually increased and the degrees of partial melting decreased and so, chemical composition of the magmas changed from tholeiitic to alkaline.. Therefore, the geochemical variations of the Gol-e-Gohar metabasites can be attributed to factors such as different degrees of partial melting, heterogeneity of mantle source, crustal thickening and contamination. In other words, the geochemical and Sr and Nd isotopic data in this work, can provide evidence of crustal extension and magmatism at early Palaeozoic in the southern Sanandaj-Sirjan metamorphic zone.

As stated by some authors, at the lower Palaeozoic era, aborted intra-continental rifts formed in the southern Sanandaj-Sirjan metamorphic zone and continued by opening of the Neo-Tethyan ocean in the middle Permian (Sheikholeslami *et al*., 2003; Fatehi, 2018) and the ocean developed until the early Triassic. Afterwards, subduction of the Neo-Tethyan lithosphere started beneath the central Iranian microcontinent.Thermobarometric estimations in the studied metabasite suggest that in the south-east of Sanandaj-Sirjan metamorphic zone the beginning of the subduction characterised by the formation of amphibolite facies rocks and deformed structures. The absence of high pressure-low temperature rock associations indicate that in this region, metamorphic events have been occurred in medium-temperature and -pressure conditions. Progressive increasing of temperature and pressure, in the studied rocks would be matched with crustal thickening and subduction by which a large volume of the crust buried and this is typically a feature of the arc-related environment (Kryza and Pin, 2002) which had been dominated at the time of formation of the metabasites. All evidences show that during the early Cimmerian orogenic phase, southern Iranian margin was an active continental margin environment.

CONCLUSIONS

Geochemical and pertographical studies shown that parent rocks of metabasites in the Gol-e-Gohar metamorphic Complex, were basaltic to andesitic lava flows and gabbroic intrusive bodies with tholeiitic to alkaline affinity. Besides, geothermobarometric calculations of the

peak metamorphic conditions yield temperatures of 640-680ºC and pressures of 7–10.5kbar (amphibolite facies) for the metabasites which is typically a feature of the arc-related environment associated with crustal thickening and coincide with the early Cimmerian orogenic phase.

i) The metabasites of the Gol-e-Gohar metamorphic Complex, (layered metamorphosed lava flows and younger metamorphosed gabbro intrusions) show different chemical compositions.

ii) The parent rocks of most metabasites from the Gol-e-Gohar metamorphic Complex (south-eastern of Sanandaj -Sirjan metamorphic zone) were basaltic to andesitic lava flows with tholeiitic affinity. These rocks show a clear layering structure and according to P-T estimations, they have been metamorphosed at temperatures of about 640º to 680ºC and pressures of 7 to 10.5kbar (amphibolite facies) in the early Cimmerian orogenic phase.

iii) The relatively flat patterns in chondrite-normalized REE and multi-elemental diagrams and lack of high depletion in HREE and HFSE contents in the studied metabasites, along with isotopic data, indicate that the primary magmas of metabasites have been derived from subcontinental lithospheric mantle with spinel-lherzolitic composition. Chemical evidence shows that the source rocks have been affected by small degrees of partial melting in an intra-continental extensional rifting environment.

iv) Some of the Gol-e-Gohar metabasites originated from gabbro intrusions. They are clearly younger than the layered metabasites and their chemical composition is similar to the continental within-plate alkali basalts, whereas layered Gol-e-Gohar metabasites have intra-continental tholeiitic affinity. We propose that during the continental rifting period in the Palaeozoic Era in the Iranian platform, at first, tholeiitic magmas were formed due to high degrees of partial melting, and then, gradually, the rate of magma generation decreased and parent alkaline magmas of gabbro intrusions formed.

v) Enrichment of the studied metabasites in TiO_2 (with a mean value of 2.16wt.%), the alternation of metabasite layers with metamorphosed sedimentary rocks, high Zr/Y ratios (between 3 to 8), tendency of the studied samples into the intra-continental rifting areas, along with the occurrence of mafic volcanism at the Palaeozoic era in Iran, indicate that at that time continental rifting and related processes occurred in the Iranian Platform.

ACKNOWLEDGMENTS

The authors thank Prof. N. Kuzuo at Yamagata University in Japan for performing electron microprobe analyses and Prof. J.F. Santos for carrying out Sr and Nd isotope analyses in the Isotope Geological Laboratory at Aveiro University (Portugal). This work was financially supported by Shahid Bahonar University of Kerman.

REFERENCES

Agard, P., Omrani, J., Jolivet, L., Mouthereau, F., 2005. Convergence history across Zagros (Iran): constraints form collisional and earlier deformation. International Journal of Earth Sciences, 94(3), 401-419.

Agard, P., Omrani, J., Jolivet, L., Whitechurch, H., Vrielynck, B., Spakmam, W., Monie, P., Meyer, B., Wortel, R., 2011. Zagros Orogeny: a subduction-dominated process. Geological Magazine, 148(5-6), 692-725.

Ahmadi Khalaji, A., Esmaeily, D., Valizadeh, M.V., Rahimpour-Bonab, H., 2007. Petrology and geochemistry of the granitoid complex of Boroujerd, Sanandaj-Sirjan Zone, western Iran. Journal of Asian Earth Sciences, 29(5-6), 859-877.

Aldanmaz, E., Pearce, J.A., Thirlwall, M.F., Mitchell, J.G., 2000. Petrogenetic evolution of Late Cenozoic Post-collision Volcanism in Western Anatolia. Turkey. Journal of Volcanology and Geothermal Research, 102(1-2), 67-95.

Aldanmaz, E., Köprübaşı, Ö.F., Gürer., Kaymakçı, N., Gourgand, A., 2006. Geochemical constrains on the Cenozoic, OIB-type alkaline volcanic rocks of NW Turkey: Implications for mantle sources and melting processes. Lithos, 86, 50-76.

Arfania, R., Shahriari, S., 2009. Role of southeastern Sanandaj-Sirjan Zone in the tectonic evolution of Zagros Orogenic Belt, Iran. Island Arc, 18(4), 555-576.

Árkai, P., Mata, M.P., Giorgetti, G., Peacor, D.R., Tóth, M., 2002. Comparison of diagenetic and low-grade metamorphic evolution of chlorite in associated metapelites and metabasites: an integrated TEM and XRD study. Journal of Metamorphic Geology, 18(5), 531-550.

Baharifar, A., Moinevaziri, H., Bellon, H., Pique, A., 2004. The crystalline complexes of Hamadan (Sanandaj-Sirjan zone, western Iran): metasedimentary Mesozoic sequences affected by Late Cretaceous tectono-metamorphic and plutonic events. Comptes Rendus Geoscience, 336(16), 1443-1452.

Best, M.G., 2002. Igneous and metamorphic petrology. Wiley-Blackwell publications, 752pp.

Bruand, E., Gasser, D., Bonnand, P., Stuewe, K., 2011. The petrology and geochemistry of a metabasite belt along the southern margin of Alaska. Lithos, 127(1-2), 282-297.

Coban, H., 2007. Basalt magma genesis and fractionation in collision and extension related provinces: A comparison between Eastern, Central and Western Anatolia. Earth-Science Reviews, 80(3), 219-238.

Droop, G.T.R., 1987. A general equation for estimating Fe^{3+} concentrations in ferromagnesian silicates and oxides from microprobe analyses, using stoichiometric criteria. Mineralogical Magazine, 51(361), 431-450.

Ellam, R.M., Cox, K.G., 1991. An interpretation of Karoo picrate basalts in terms of interaction between asthenospheric

magmas and the mantle lithosphere. Earth and Planetary Science Letters, 105(1-3), 330-342.

Fatehi, H., unpublished. Mineralogy, geochemistry and petrogenesis of metamorphic rocks in Gol-e-Gohar and Rutchun complexes (southwest of Baft city, Kerman province) (in persian). Doctoral Thesis. Shahid Bahonar, University of Kerman, 404pp.

Fatehi, H., Ahmadipour, H., Kuzuo, N., Moeinzadeh, H., 2017. Feather-like hornblende aggregates in the phyllites from the southern Sanandaj–Sirjan zone, Iran; their origin and mode of formation. Turkish Journal of Earth Sciences, 26(6), 421-440.

Fitton, J.G., Saunders, A.D., Norry, M.J., Hardarson, B.S., Taylor, R.N., 1997. Thermal and chemical structure of the Iceland plume. Earth and Planetary Science Letters, 153(3-4),197-208.

Frey, F.A., 1982. Rare Earth Element Abundances in Upper Mantle Rocks. In: Henderson, P. (ed.). Rare Earth Element Geochemistry, 2, 153-203. DOI: 10.1016/B978-0-444-42148-7.50010-1

Frey, F.A., Garcia, M.O., Wise, W.S., Kennedy, A., Gurriet, P., Albarede, F., 1991. The evolution of Mauna Kea volcano, Hawaii: petrogenesis of tholeiitic and alkalic basalts. Journal of Geophysical Research, 96(B9), 14347-14375.

Ghalamghash, J., Nèdèlec, A., Bellon, H., Vousoughi Abedini, M., Bouchez, J.L., 2009. The Urumieh plutonic complex (NW Iran): A record of the geodynamic evolution of the Sanandaj-Sirjan zone during Cretaceous times - Part I: Petrogenesis and K/Ar dating. Journal of Asian Earth Sciences, 35(5), 401-415.

Gower, C.F., Swinden, H.S., 1991. Pillow lavas in the Dead Islands area, Grenville province, southeast Labrador. Current Research, New Found Land Department of Mines and Energy, Geological Survey Branch, Report 91(1), 205-215.

Hart, W.K., Wolde, G.C., Walter, R.C., Mertzman, S.A., 1989. Basaltic volcanism in Ethiopia: constraints on continental rifting and mantle interactions. Journal of Geophysical Research, 94, 7731-7748.

Holland, T., Blundy, J., 1994. Non-ideal interactions in calcic amphiboles and their bearing on amphibole-plagioclase thermometry. Contributions to Mineralogy and Petrology, 116(4), 433-447.

Jung, S., Hoernes, S., 2000. The major and trace element and isotope (Sr, Nd, O) geochemistry of Cenozoic alkaline rift-type volcanic rocks from the Rhön area (central Germany): petrology, mantle source characteristics and implications for asthenosphere lithosphere interactions. Journal of Volcanology and Geothermal Research, 99(1-4), 27-53. DOI: 10.1016/S0377-0273(00)00156-6

Kapp, P., Manning, C.E., Tropper, P., 2009. Phase-equilibrium constraints on titanite and rutile activities in mafic epidote amphibolites and geobarometry using titanite–rutile equilibria. Journal of Metamorphic Geology, 27(7), 509-521.

Khudoley, A.K., Prokopiev, A.V., Chamberlain, K.R., Ernst, R.E., Jowitt, S.M., Malyshev, S.V., Zaitsev, A.I., Kropachev, A.P., Koroleva, O.V., 2013. Early Palaeozoic mafic magmatic events on the eastern margin of the Siberian Craton. Lithos, 174, 44-56.

Kryza, R., Pin, C., 2002. Mafic rocks in a deep-crustal segment of the Variscides (the Góry Sowie, SW Poland): evidence for crustal contamination in an extensional setting. International Journal of Earth Science, 91(6), 1017-1029.

Leake, B.E., Woolley, A.R., Arps, C.E.S., Birch, W.D., Gilbert, M.C., Grice, J.D., Hawthorne, F.C., Kato, A., Kisch, H.J., Krivovichev, V.G., Linthout, K., Laird, J., Mandarino, J.A., Lucassen, F., Franz, G., Romer, R.L., pudlo, D., Dulski, P., 2008. Nd, Pb and Sr isotope composition of Late Mesozoic to Quaternary intra-plate magmatism in NE- Africa (Sudan, Egypt): high-μ signatures from the mantle lithosphere. Contributions to Mineralogy and Petrology, 156(6) ,756-784. DOI: 10.1007/s00410-008-0314-0

Mahmoodi, S.H., Corfu, F., Masoudi, F., Mehrabi, B., Mohajjel, M., 2011. U-Pb dating and emplacement history of granitoid plutons in the northern Sanandaj-Sirjan Zone, Iran. Journal of Asian Earth Sciences, 41(3), 238-249.

Maruyama, S., Liou, J.G., Terabayashi, M., 1996. Blueschists and eclogites of the world and their exhumation. International Geology Review, 38(6), 485-596. DOI: 10.1080/00206819709465347

Meschede, M., 1986. A method of discriminating between different types of mid-ocean ridge basalts and continental tholeiites with the Nb- Zr- Y diagram. Chemical Geology, 56(3-4), 207-218.

Mohajjel, M., Fergusson, C.L., 2000. Dextral transpression in late Cretaceous continental collision, Sanandaj-Sirjan Zone, western Iran. Journal of Structural Geology, 22(8), 1125-1139.

Mohajjel, M., Fergusson, C.L., 2014. Jurassic to Cenozoic tectonics of the Zagros Orogen in the northwestern Iran. International Geology Reviews, 56(3), 263-287.

Mohajjel, M., Fergusson, C.L., Sahandi, M.R., 2003. Cretaceous-Tertiary convergence and continental collision, Sanandaj-Sirjan Zone, western Iran. Journal of Asian Earth Sciences, 21(4), 397-412.

Mohajjel, M., Baharifar, A., Moinevaziri, H., Nozaem, R., 2006. Deformation history, micro-structure and P-T-t path in ALS bearing schist, southeast Hamadan, Sanandaj-Sirjan Zone, Iran. Journal of Geological Society of Iran, 1, 11-19.

Nagudi, N., Koberl, Ch., Kurat, G., 2003. Petrography and geochemistry of the Singo granite, Uganda, and implications for its origin. Journal of African Earth Sciences, 36, 73-87.

Nakamura, N., 1974. Determination of REE, Ba, Fe, Mg, Na and K in carbonaceous and ordinary chondrite. Geochimica et Cosmochimica Acta, 38(5), 757-775.

Oliveros, V., Morata, D., Aguirre, L., Feraud, G., Fornari, M., 2007. Jurassic to Early Cretaceous subduction-related magmatism in the Coastal Cordillera of northern Chile (18º30'-24ºS): geochemistry and petrogenesis. Revista Geológica de Chile, 34, 209-232. DOI: 10.4067/S0716-02082007000200003

Omrani, J., Agard, P., Whitechurch, H., Benoit, M., Prouteau, G., Jolivet, L., 2008. Arc-magmatism and subduction history beneath the Zagros Mountains, Iran: A new report of adakites geodynamic consequences. Lithos, 106(3-4), 380-398.

Otten, M.T., 1984. The origin of brown hornblende in the Artfjället gabbro and dolerite. Contributions to Mineralogy and Petrology, 86(2), 189-199.

Pearce, J.A., 1983. Roll of the sub-continental lithosphere in magma genesis at active continental margins. In: Hawkesworth, C.J., Norry, M.J. (eds.). Continental basalts and mantle xenoliths. Nantwich, Shiva, 230-249.

Pearce, J.A., 2008. Geochemical fingerprinting of oceanic basalts with applications to ophiolite classification and the search for Archean oceanic crust. Lithos, 100(1-4), 14-48.

Pearce, J.A., Cann, J.R., 1973. Tectonic setting of basic volcanic rocks determined using trace element analyses. Earth and Planetary Science Letters, 19(2), 290-300.

Pearce, J.A., Norry, M.J., 1979. Petrogenetic implications of Ti, Zr, Y, Nb variations in volcanic rocks. Contributions to Mineralogy and Petrology, 69(1), 33-47.

Pearce, J.A., Peate, D.W., 1995. Tectonic implications of the composition of volcanic arc magmas. Annual Review of Earth and Planetary Sciences, 23, 251-285.

Pearce, J.A.A., Baker P.E., Harvey P.K., Luff I.W., 1995. Geochemical evidence for subduction fluxes, mantle melting and fractional crystallization beneath the South Sandwich island arc. Journal of Petrology, 36(4), 1073-1109.

Pe-Piper, G., 1988. Calcic amphiboles of mafic rocks of the Jeffers Brook plutonic complex, Nova Scotia, Canada. American Mineralogist, 73, 993-1006.

Peters, T.G., Menzies, M., Thitlwall, M., Kyle, P.K., 2008. Zuni-Bandera volcanism, Rio Grande, USA, Melt formation in garnet- and spinel-facies mantle straddling the asthenosphere-lithosphere boundary. Lithos, 102(1-2), 295-315.

Rickwood, P.C., 1989. Boundary lines within petrologic diagrams which use oxides of major and minor elements. Lithos, 22(4), 247-263.

Robinson, P., Spear, F.S., Schumacher, J.C., Laird, J., Klein, C., Evans, B.W., Doolan, B.L., 1982. Phase relations of metamorphic amphiboles: Natural occurrences and theory. In: Veblen, D.R., Ribbe, P.H. (eds.). Amphiboles: Petrology and Experimental Phase Relations. Mineralogical Society of America, Reviews in Mineralogy, 98, 1-228.

Rolland, Y., Pecher, A., Picard, C., 2000. Middle Cretaceous back-arc formation and arc evolution along the Asian margin: the Shoyk Suture Zone in northern Ladakh (NW Himalaya). Tectonophysics, 325(1-2), 145-173.

Rollinson, H.R., 1996. Using Geochemical Data: Evaluation, Presentation, Interpretation. Singapore, Longman Geochemistry Series, 325pp.

Sabzehei, M., Navazi, M., Azizan, H., Roshan Ravan, J., Nazemzadeh, M., 1997. Geological Map of Khabr. 1:100,000. Geological Survey of Iran, Teheran, Iran.

Saki, A., Moazzen, M., Oberhänsli, R., 2011. P–T evolution of the Precambrian Metamorphic Complex, NW Iran: a study of metapelitic rocks. Geological Journal, 46(1),10-25.

Schandl, E.S., Gorton, M.P., 2002. Application of high field strength elements to discriminate tectonic setting in VMS environments. Economic Geology, 97(3), 629-642.

Schmidt, M.W., 1992. Amphibole composition in tonalite as a function of pressure: an experimental calibration of the Al-in-hornblende barometer. Contributions to Mineralogy and Petrology, 110(2-3), 304-310.

Sepahi, A.A., Whitney, D.L., Baharifar, A.A., 2004. Petrogenesis of andalusite-kyanite-sillimanite veins and host rocks, Sanandaj-Sirjan metamorphic belt, Hamadan, Iran. Journal of Metamorphic Geology, 22(2), 119-134.

Sheikholeslami, R., Bellon, H., Emami, H., Sabzehei, M., Pique, A., 2003. Nouvelles donnees structurales et datations ^{40}K-^{40}Ar sur les roches metamorphiques de la region de Neyriz (Zone de Sanandaj-Sirjan, Iran meridional). Leur interet dans le cadre du domaine neo-tethysien du Moyen-Orient (in french). Compres rendus Geoscience, 335(13), 981-991. DOI: 10.1016/j.crte.2003.09.001

Sheikholeslami, M.R., Pique, A., Mobayen, P., Sabzehi, M., Bellon, H., Emami, M.H., 2008. Tectono-metamorphic evolution of the Neyriz metamorphic complex, Quri-Kor-e-sefid area (Sanandaj-Sirjan zone, SW Iran). Journal of Asian Earth Sciences, 31(4-6), 504-521.

Stocklin, J., 1968. Structural History and Tectonics of Iran: A Review. American Association of Petroleum Geologists Bulletin, 52(7), 1229-1258.

Sun, S.S., McDonough, W.F., 1989. Chemical and isotopic systematic of oceanic basalts: implications for mantle composition and processes. In: Saunders, A.D., Norry, M.J. (eds.). Magmatism in the Ocean Basins. Geological Society Special Publication, 42, 313-345.

Taylor, S.R., McLennan, S.M, 1985. The Continental Crust: its Composition and Evolution. Oxford, Blackwell Scientific Publication, 312pp.

Verma, S.P., 2009. Continental Rift Setting for the Central Part of Mexican Volcanic Belt: A Statistical Approach. The Open Geology Journal, 3, 8-29.

Whitney, D.L., Evans, B.W., 2010. Abbreviation for names of rock-forming minerals. American Mineralogist, 95(1), 185-187.

Widdowson, M., Pringle, M.S., Fernandez, O.A., 2000. A post K-T Boundary (Early Paleocene) age for Deccan-type feeder dykes, Goa, India. Journal of Petrology, 41(7), 1177-1194.

Will, M.T., Frimmel, E.F., Gaucher, C., Bossi, J., 2014. Geochemical and isotopic composition of Pan-African metabasalts from southwestern Gondwana: Evidence of Cretaceous South Atlantic opening along a Neoproterozoic back-arc. Lithos, 202-203, 363-381.

Wilson, M., 1989, Igneous Petrogenesis. A Global Tectonic Approach. London, Unwin Hyman, 466pp.

Winchester, J.A., Floyd, P.A., 1977. Geochemical discrimination of different magma series and their differentiation products using immobile elements. Chemical Geology, 20, 325-343.

Wones, D.R., Eugster, H.P., 1965. Stability of biotite: experimental, theory and application. The American Mineralogist, 50(9), 1228-1272.

Zindler, A., Hart, S., 1986. Chemical geodynamics. Annual Review of Earth and Planetary Sciences, 14, 493-571.

Manuscript received February 2017;
revision accepted May 2018;
published Online July 2018.